

Supplementary information

Systems-level effects of allosteric perturbations to a model molecular switch

In the format provided by the
authors and unedited

Systems-level effects of allosteric perturbations to a model molecular switch – Supplementary File

Tina Perica^{1, 2, 3,12}, Christopher J. P. Mathy^{1, 2, 4,12}, Jiewei Xu^{2, 5, 6}, Gwendolyn M. Jang^{2, 5, 6}, Yang Zhang^{1, 2}, Robyn Kaake^{2, 5, 6}, Noah Ollikainen^{1, 2, 7}, Hannes Braberg^{2, 5, 6}, Danielle L. Swaney^{2, 5, 6}, David G. Lambright^{8,9}, Mark J. S. Kelly¹⁰, Nevan J. Krogan^{2, 5, 6*}, Tanja Kortemme^{1, 2, 4, 7, 11*}

¹ Department of Bioengineering and Therapeutic Sciences, University of California San Francisco, San Francisco, CA, USA

² Quantitative Biosciences Institute (QBI), University of California San Francisco, San Francisco, CA, USA

³ European Molecular Biology Laboratory, European Bioinformatics Institute (EMBL-EBI), Cambridge, UK.

⁴ The UC Berkeley-UCSF Graduate Program in Bioengineering, University of California San Francisco, San Francisco, CA, USA

⁵ Department of Cellular and Molecular Pharmacology, University of California San Francisco, San Francisco, CA, USA

⁶ The J. David Gladstone Institutes, San Francisco, CA, USA.

⁷ Graduate Program in Bioinformatics, University of California San Francisco, San Francisco, California, United States of America.

⁸ Program in Molecular Medicine, University of Massachusetts Medical School, Worcester, MA 01605, USA.

⁹ Department of Biochemistry and Molecular Pharmacology, University of Massachusetts Medical School, Worcester, MA 01605, USA.

¹⁰ Department of Pharmaceutical Chemistry, University of California, San Francisco, San Francisco, CA 94143, USA.

¹¹ Chan Zuckerberg Biohub, San Francisco, California.

¹² These authors contributed equally

* Correspondence: kortemme@cgl.ucsf.edu, nevan.krogan@ucsf.edu

TABLE OF CONTENTS

| | |
|---|----|
| SUPPLEMENTARY DISCUSSION..... | 5 |
| LINKAGE CRITERIA USED FOR E-MAP HIERARCHICAL CLUSTERING ANALYSES..... | 5 |
| POTENTIAL DEPENDENCIES BETWEEN ALLELES WHEN COMPUTING GENETIC INTERACTION (GI) PROFILE CORRELATIONS | 6 |
| ROBUSTNESS OF THE ANALYSIS TO LEAVING OUT DATA..... | 9 |
| POTENTIAL CAVEATS ASSOCIATED WITH USING THE GAP (RNA1) FROM S. POMBE..... | 13 |
| VALIDITY OF THE MICHAELIS-MENTEN FORMALISM FOR GTPASES..... | 15 |
| SUPPLEMENTARY METHODS..... | 17 |
| POINT MUTATIONS IN GENOMIC Gsp1 SEQUENCE | 17 |
| S. CEREVIAE GENETICS AND GENETIC INTERACTION MAPPING | 18 |
| <i>S. cerevisiae transformation</i> | 18 |
| <i>Epistatic mini-array profiling (E-MAP) of Gsp1 point mutants</i> | 19 |
| <i>Hierarchical clustering of E-MAP genetic interaction data</i> | 20 |
| <i>Scaling of published genetic interaction data to the E-MAP format</i> | 20 |
| <i>Significance of genetic interactions</i> | 21 |
| <i>GI profile correlation measurements</i> | 22 |
| <i>Protein expression levels by Western Blot</i> | 24 |
| PHYSICAL INTERACTION MAPPING USING AFFINITY PURIFICATION MASS SPECTROMETRY (AP-MS)..... | 26 |
| <i>S. cerevisiae cell lysate preparation</i> | 26 |
| <i>FLAG immunoprecipitation</i> | 27 |
| <i>Liquid chromatography with tandem mass spectrometry (LC-MS/MS) analysis</i> | 28 |
| BIOCHEMICAL AND BIOPHYSICAL ASSAYS | 29 |
| <i>Protein purifications</i> | 29 |
| <i>Circular dichroism (CD) spectroscopy of protein thermostability</i> | 31 |
| <i>GTP loading of Gsp1</i> | 32 |
| <i>Reverse phase high performance liquid chromatography (HPLC)</i> | 32 |
| <i>NMR Spectroscopy</i> | 33 |

| | |
|--|-----------|
| <i>Kinetic measurements of GTP hydrolysis.</i> | 34 |
| <i>Estimating the k_{cat} and K_m parameters of GAP-mediated hydrolysis using an accurate solution to the integrated Michaelis-Menten equation.</i> | 35 |
| <i>Kinetic measurements of Srm1 mediated nucleotide exchange.</i> | 38 |
| SUPPLEMENTARY FIGURES..... | 41 |
| <i>Supplementary Figure 1 Cartoon representation of co-complex structures of <i>S. cerevisiae</i> Gsp1 (dark navy) with indicated partners (or homologs).</i> | 41 |
| <i>Supplementary Figure 2 Comparison of definitions of high confidence S-scores used in our analysis.</i> | 42 |
| <i>Supplementary Figure 3 GAP-mediated GTP hydrolysis monitored as fluorescence increase upon binding of released free phosphate to a fluorescent phosphate sensor.</i> | 45 |
| <i>Supplementary Figure 4 Michaelis-Menten plots for GEF-mediated nucleotide exchange.</i> | 48 |
| <i>Supplementary Figure 5 Schematic of genetically integrated GSP1 constructs.</i> | 49 |
| <i>Supplementary Figure 6 Reproducibility of GSP1 point mutant E-MAP screens.</i> | 50 |
| <i>Supplementary Figure 7 Clustering of individual AP-MS replicates based on correlations between protein abundance before the final scoring.</i> | 51 |
| <i>Supplementary Figure 8 Clustering of individual AP-MS replicates based on correlations between protein abundance before the final scoring.</i> | 52 |
| <i>Supplementary Figure 9 Multiple sequence alignment between Rna1 from <i>S. cerevisiae</i> (Rna1_YEAST) and <i>S. pombe</i> (Rna1_SCHPO), as well as human RanGAP (RAGP1_HUMAN, excluding the C-terminal SUMO conjugation domain which is absent in Fungi).</i> | 53 |
| <i>Supplementary Figure 10 Non-linear scaling of SGA data from the Cell Map to E-MAP format.</i> | 54 |
| <i>Supplementary Figure 11 Example data for Gsp1 protein expression estimation by Western blot.</i> | 55 |
| <i>Supplementary Figure 12 Silver stain gels after FLAG immunoprecipitation of amino- (N) or carboxy- (C) terminally 3xFLAG tagged genetically integrated Gsp1.</i> | 56 |
| <i>Supplementary Figure 13 Circular dichroism (CD) data for wild type (WT) Gsp1 and select mutants.</i> | 57 |
| <i>Supplementary Figure 14 HPLC reverse phase chromatograms of a GTP/GDP mix (top) and that of a purified and GTP loaded wild type Gsp1 (bottom).</i> | 58 |

| | |
|--|-----------|
| <i>Supplementary Figure 15 Accuracy estimation for determining the kinetic parameters of GAP-mediated GTP hydrolysis from individual time courses spanning [S] > Km to [S] << Km fit with an accurate solution of the integrated Michaelis-Menten (IMM) equation.</i> | 59 |
| <i>Supplementary Figure 16 Estimated error around the maximum likelihood estimated values of the Michaelis-Menten parameters.</i> | 60 |
| SUPPLEMENTARY TABLES | 62 |
| <i>Supplementary Table 1 Co-complex X-ray crystal structures of Ran or Gsp1 with its partners.</i> | 62 |
| <i>Supplementary Table 2 Mutated residues in Gsp1 and their interface position and ΔrASA</i> | 63 |
| <i>Supplementary Table 3 Gsp1 mutants and attempted yeast constructs.</i> | 66 |
| <i>Supplementary Table 4 Pearson correlations between Gsp1 mutants and the alleles of their direct interaction partners from the SGA CellMap.</i> | 69 |
| <i>Supplementary Table 5 Interquartile range (IQR) of log₂(fold change) values across all the Gsp1 mutants for each prey protein identified.</i> | 73 |
| <i>Supplementary Table 6 Michaelis-Menten parameters of GAP-mediated GTP hydrolysis.</i> | 76 |
| <i>Supplementary Table 7 Michaelis-Menten parameters of GEF-mediated nucleotide exchange.</i> | 77 |
| <i>Supplementary Table 8 Intrinsic GTP hydrolysis rate of wild type and mutant Gsp1.</i> | 78 |
| <i>Supplementary Table 9 Apparent T_m values estimated from the circular dichroism (CD) thermal melts.</i> .. | 79 |
| TITLES AND LEGENDS OF SUPPLEMENTARY SOURCE FILES..... | 80 |
| <i>SOURCE FILE 1 GENETIC INTERACTION (GI) DATA FROM THE E-MAP SCREENS.....</i> | 80 |
| <i>SOURCE FILE 2 PAIRWISE PEARSON CORRELATIONS OF PROFILES BETWEEN SGA GENES AND GSP1 POINT MUTANTS, WITH ASSOCIATED P-VALUES.</i> | 81 |
| <i>SOURCE FILE 3 AFFINITY PURIFICATION MASS SPECTROMETRY (AP-MS) DATA REPORTED AS FOLD CHANGE AND SIGNIFICANCE VALUE, AS WELL AS A LIST OF SIGNIFICANT INTERACTION HITS.</i> | 82 |
| <i>SOURCE FILE 4 S. CEREVIAE GENES FROM THE SGA DATA WITH SIGNIFICANT POSITIVE CORRELATIONS WITH GSP1 MUTANTS ORGANIZED BY BIOLOGICAL FUNCTIONS INTO GENE SETS.</i> | 84 |
| SUPPLEMENTARY REFERENCES | 85 |

Supplementary Discussion

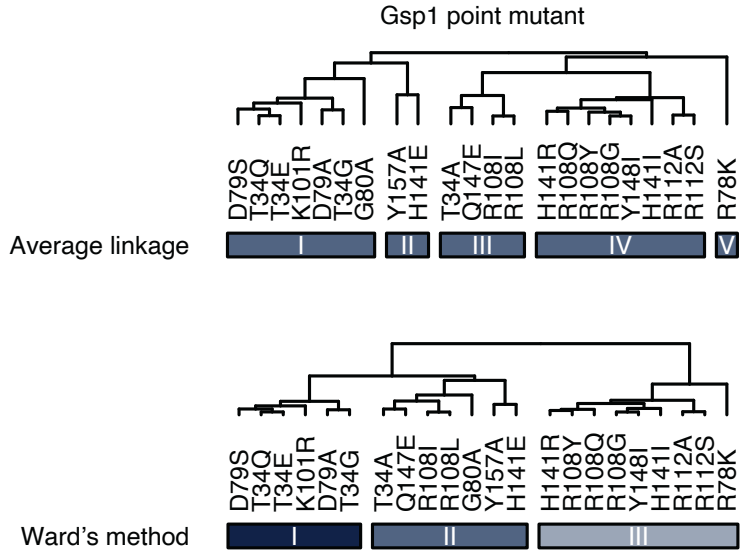
Linkage criteria used for E-MAP hierarchical clustering analyses

For clustering of Gsp1 mutants and E-MAP library genes (in **Fig. 1c**, **Extended Data Figs. 3 and 4b**) we used average linkage to be consistent with how we and others have clustered and represented genetic interaction (GI) data in previously published E-MAP datasets (as detailed in: Ref⁴²). Even though our data are based on screens of point mutants of a single protein, different from most previous studies that screen knockouts of many different genes, we show that average linkage remained an appropriate criterion for clustering our E-MAP matrix based on the recovery of known groups of functionally related genes within the dendrogram of library genes (**Fig. 1c** and **Extended Data Fig. 4b**).

The clustering analysis in **Fig. 4a** had the goal to assign the Gsp1 mutants by functional similarity to classes in an unbiased manner, and to assess whether the classes of mutants matched the grouping defined by the *in vitro* kinetics and NMR data. To quantify functional similarity, we adopted the widespread approach of computing correlation coefficients between GI profiles. Most studies have represented these data as networks and used existing annotations (typically Gene Ontology categories) to assert functional groupings¹⁴ but we sought to use an unsupervised clustering approach instead. To do so, we used Ward's linkage criterion, since it was designed to build hierarchies by selecting joining operations that minimize within-group dispersion⁴³ to find compact, spherical clusters. Indeed, we found Ward's linkage resulted in rounder clusters reflecting known biological functions, and these clusters were less sensitive to sparsely populated outliers. In contrast, we found the average linkage criterion to be more sensitive to a few sparsely populated outliers (resulting in a variety of group sizes).

Nonetheless, to show that the linkage method used does not alter our primary conclusions regarding the grouping of mutants, we compared the clustering from average linkage with the

clustering from Ward's method in the dendrograms shown in the Figure below. Both methods identify the three main classes of mutants (I, II, and III below, I, III, and IV above), but average linkage is more sensitive to the sparsely populated vectors and outliers, resulting in a wider variety of cluster sizes.



Hierarchical clustering of 22 strong Gsp1 point mutants by the p-value of Pearson correlations of their GI profiles and those of 276 *S. cerevisiae* alleles, using either the average linkage (top) or Ward's method (bottom) as linkage criterion.

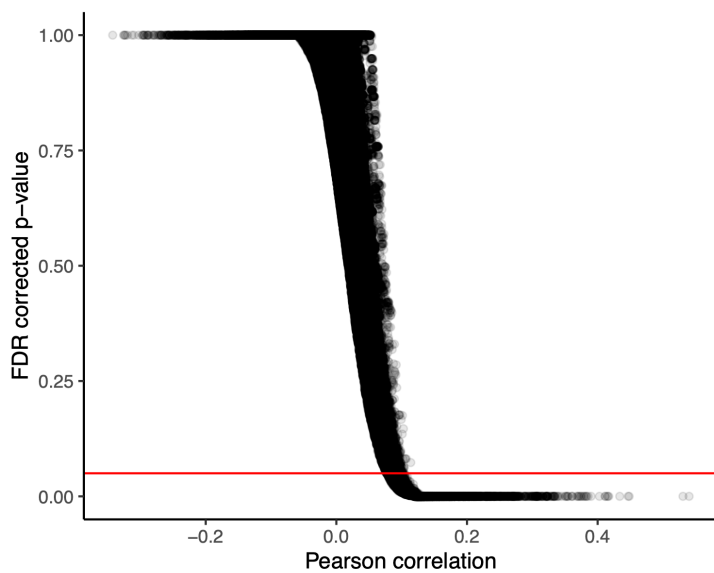
Potential dependencies between alleles when computing genetic interaction (GI) profile correlations

We use Pearson correlations in three cases: (1) as a distance metric for clustering the Gsp1 E-MAP matrix (**Fig 1c** and **Extended Data Figs. 3 and 4b**), (2) for quantifying the functional similarity of GI profiles of Gsp1 point mutants and *S. cerevisiae* alleles (**Fig 1e**, **Fig 4abd**, and **Extended Data Fig. 10**), and (3) as a distance metric for clustering the vectors of Gsp1 mutant correlations (**Fig 4a**). In all three cases, there are certainly dependencies between some *S. cerevisiae* alleles, as evidenced by their own clustering into groups according to their biological function (**Fig 1c**): mRNA export genes cluster together, meaning that if one mRNA export gene has a large negative S-score with a Gsp1 mutant, other mRNA export genes are likely to

as well (relevant for case 1). Likewise, if the GI profile of a gene is significantly correlated with a Gsp1 mutant, other genes in the same pathway are likely to have correlated profiles as well (relevant for cases 2 and 3). This dependency is expected and is indeed a main benefit of a GI profiling approach, as the S-scores allow us to infer functional relationships between genes and ascribe likely functions to unknown genes.

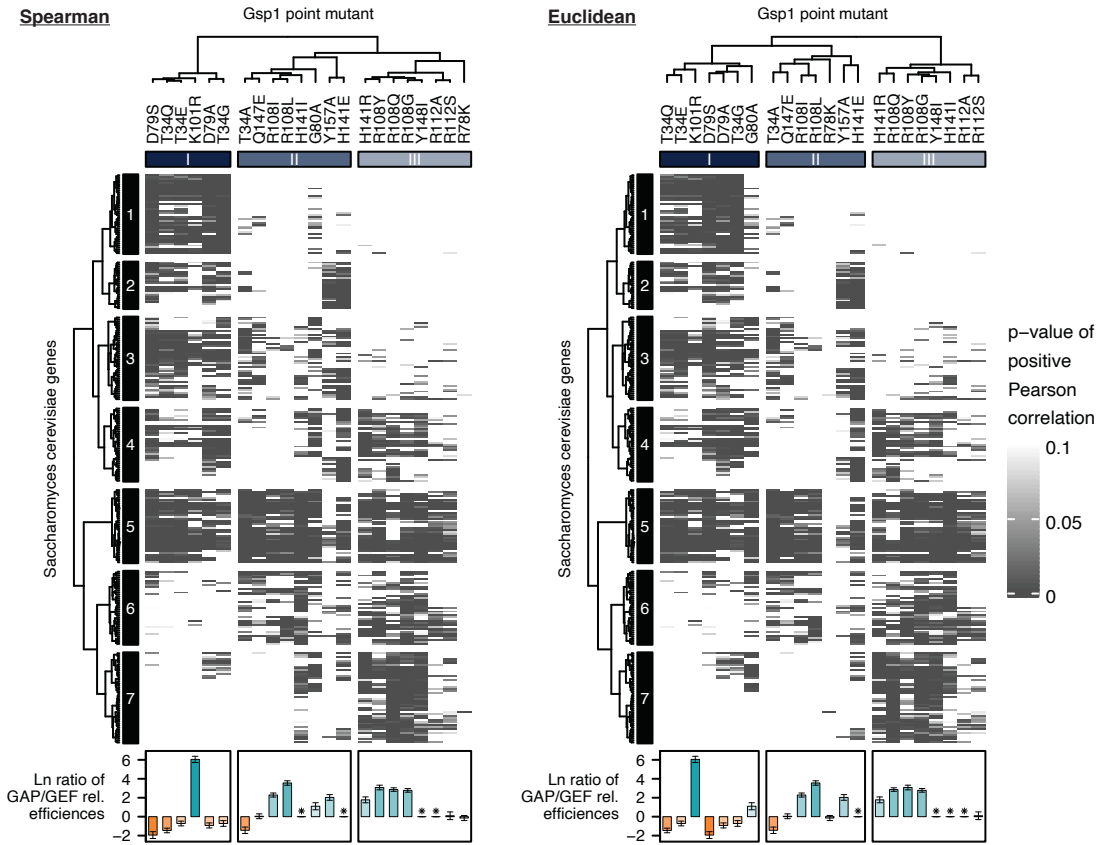
With regards to Case 1, we note that assessing similarity of GI profiles using Pearson correlations without further correction for dependencies between alleles is a standard analysis^{14,26}.

Case 2 is the only analysis for which we compute statistical significance when using correlations. We accounted for the dependencies between alleles by adjusting our p-values to control the False Discovery Rate, which has been shown to be valid when this form of dependency (positive regression dependency) exists between test statistics²⁹. In the manuscript figures we use these corrected p-values instead of correlation values for simplicity, because, as can be seen from the plot, only positive correlations of above 0.1 have significant p-values.



With regards to Case 3, most GI studies have used the correlations between GI profiles to define edge attributes for graphical representations of GI networks. We elected to keep the data

in matrix form and cluster it to identify functionally similar groups of mutants and *S. cerevisiae* alleles in an unbiased fashion. To cluster the Gsp1 vectors of p-values (columns), we used Pearson correlations as a distance metric. To cluster the *S. cerevisiae* alleles (rows), we used the Euclidean distance instead of the Pearson correlation (as stated in the *GI profile correlation measurements* section of the Methods) because the vectors were only 22 entries long and many were sparse, making them especially sensitive to outliers when using Pearson correlation as the distance metric. To test whether the use of Pearson correlations for the clustering of mutant vectors significantly changes our clustering, we re-clustered the matrix in **Fig. 4a** using the Spearman correlation or the Euclidean distance as distance metrics instead. While there are slight differences in the ordering of mutants using these different distance metrics, the grouping of mutants is very similar to the original heatmap in **Fig 4a** in that it identifies a GAP-perturbed group of mutants, a GEF-perturbed group of mutants, and an intermediate group (**Figure** below). Thus, we believe this analysis robustly identifies three functional classes of Gsp1 mutants regardless of any effect that dependencies between the *S. cerevisiae* alleles may have on the Pearson correlations.

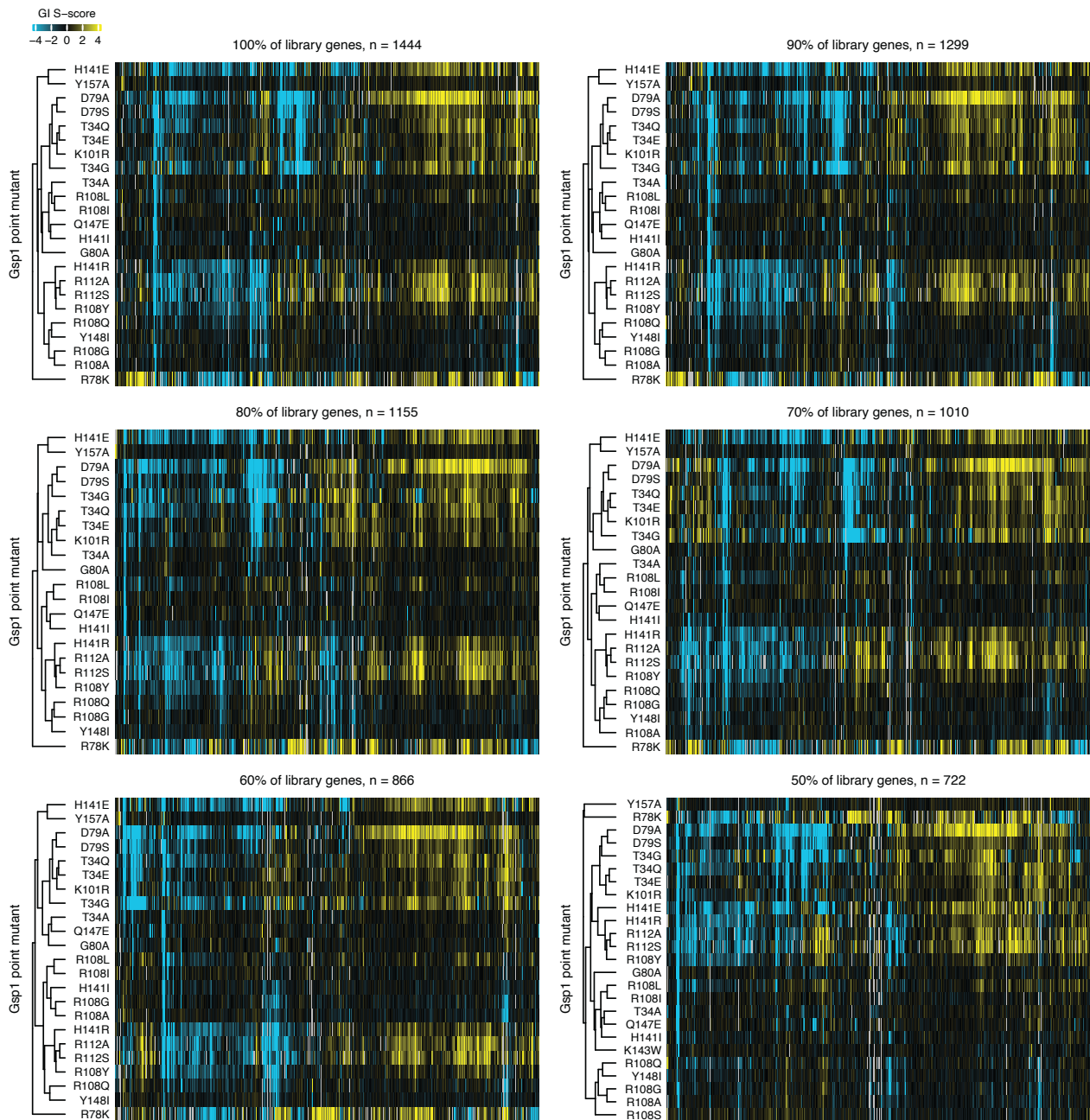


Clustering of *S. cerevisiae* alleles and strong Gsp1 point mutants by the p-value of Pearson correlations using alternative distance metrics. Hierarchical clustering of 276 *S. cerevisiae* alleles and 22 strong Gsp1 point mutants by the p-value of Pearson correlations of their GI profiles compared to the relative efficiencies of GAP-mediated GTP hydrolysis and GEF-mediated nucleotide exchange as indicated (asterisks indicate not measured). The p-value is a false discovery rate adjusted one-sided (positive) p-value of the Pearson correlations (represented as gray scale). The underlying data are identical to those presented in **Fig. 4a**, but the column clustering was performed using the Spearman correlation or the Euclidean Distance rather than the Pearson correlation as a distance metric.

Robustness of the analysis to leaving out data

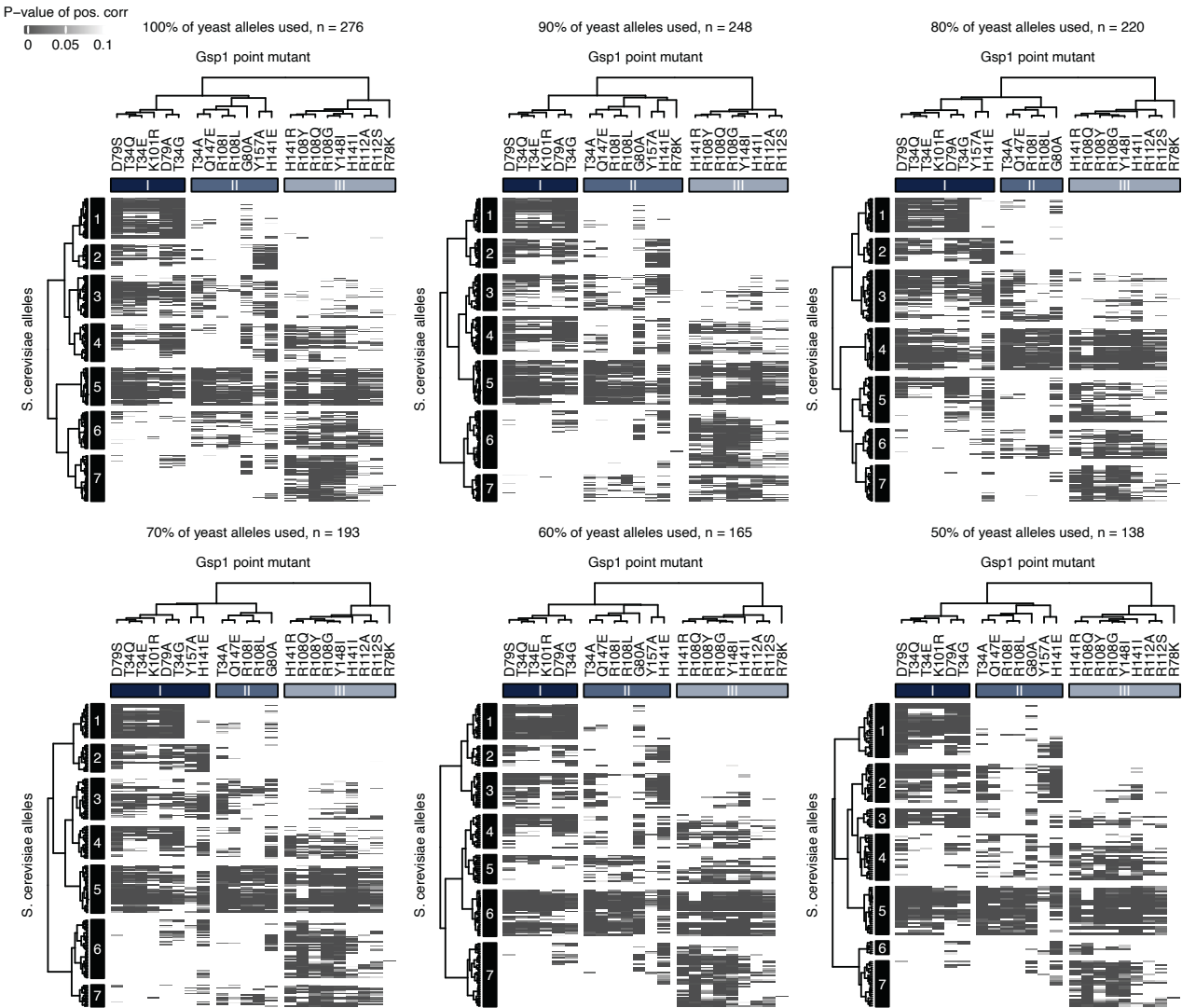
Sub-sampling EMAP data.

We randomly subsampled the library genes in the Gsp1 E-MAP (**Fig. 1c**) and found that similar groupings of mutants were maintained down to 60% of the library (**Figure below**).



Subsampling of *S. cerevisiae* alleles maintains clustering of Gsp1 mutants based on their E-MAP profiles. GI profiles of Gsp1 mutants. Negative S-score (blue) represents synthetic sick/lethal GIs, positive S-score (yellow) represents suppressive/epistatic GIs. Mutants and genes are hierarchically clustered by Pearson correlation. As in **Fig. 1c**, all 55 point mutants are included in the clustering of columns, but only the dendrogram branch containing the strong mutants is shown. The clustering of mutants is robust to subsampling, with similar ordering of mutants observed down to removal of at least 60% of library genes.

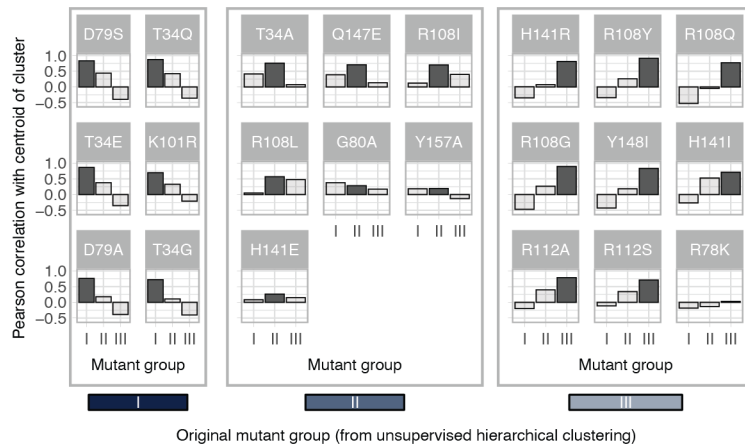
We also sub-sampled the *S. cerevisiae* alleles in the correlation p-value matrix (**Fig. 4a**) and found that the groupings of mutants were maintained down to 50% (**Figure** below).



Random subsampling of *S. cerevisiae* alleles maintains clustering of Gsp1 mutants based on the p-value of Pearson correlations of their GI profiles. The p-value is a false discovery rate adjusted one-sided (positive) p-value of the Pearson correlations (represented as gray scale). The grouping of mutants into the three observed groups is robust to subsampling, as the groups are maintained down to removal of at least 50% of alleles.

Withholding mutants

We performed a computational analysis where we withheld each of our mutants from the analysis one at a time, perform the clustering of genetic interaction profiles for the remaining data as in **Fig.4a**, and then assign the withheld mutant to the group whose centroid is most correlated with the mutant. The Figure below shows that in 21/22 cases, the withheld mutant had the highest correlation with the centroid of its original group (dark bars). This analysis confirms the robustness of our analysis and addresses the question whether our model would be capable of placing a new mutant not included in the analysis into the correct category.



Leave-one-out analysis of Fig. 4a: Each bar graph shows the Pearson correlation values between the indicated withheld mutant and the centroid of each of the three groups identified by hierarchical clustering of the remaining 21 mutants. We grouped the bar graphs according to the original group to which each mutant was assigned in **Fig. 4a**. For each of the withheld mutants, the dark bar represents the expected group (group I left bar, group II middle bar, group III right bar). With the exception of G80A, which is slightly more correlated with the group I centroid (Pearson correlation = 0.38) than the centroid of its original group, group II (Pearson correlation = 0.28), all other mutants have the highest correlation with their original groups.

Potential caveats associated with using the GAP (Rna1) from *S. pombe*

Our GAP-mediated GTP hydrolysis kinetics experiments used the wild type and mutant Gsp1 from *S. cerevisiae*, but Rna1 GAP from *S. pombe*. We chose to use the Rna1 ortholog from *S. pombe* as *S. cerevisiae* Rna1 formed soluble aggregates after purification, and *S. pombe* Rna1 was the only RanGAP for which there was a structure in complex with Ran (PDB IDs: 1K5D and 1K5G). While there could be slight differences between the kinetic parameters of *S. pombe* and *S. cerevisiae* GAP Rna1 acting on Gsp1, we do not believe these differences would significantly affect our conclusions, based on the following considerations:

Sequence conservation between *S. cerevisiae* and *S. pombe* Rna1. A sequence alignment between *S. cerevisiae*, *S. pombe*, and human GAP proteins shows that all but one interface core residue in the PDB file 1K5D is conserved in sequence between *S. cerevisiae* and *S. pombe* (**Supplementary Fig. 9**). Overall, out of the 1290 Å² buried by *S. pombe* Rna1 upon interface formation with Ran (PDB 1K5D), 997 Å² (77%) are buried by residues that are conserved in sequence between *S. pombe* and *S. cerevisiae*, and the sequence identity of the Rna1 interface with Ran/Gsp1 (including all residues that change solvent accessible surface area upon complex formation) overall is 71% (**Supplementary Table 1**).

Comparable kinetic parameters to the human Ran/RanGAP1 pair. The kinetic parameters for our *S. cerevisiae* Gsp1 and *S. pombe* Rna1 GAP are comparable to the kinetic parameters for the human Ran and human RanGAP1 reported by Klebe *et al.*⁴¹. They estimate a K_m of 0.45 μM and k_{cat} of 2.1 s⁻¹ for Ran/RanGAP1 at 25°C, while our values for the wild type *S. cerevisiae* Gsp1 and *S. pombe* Rna1 at 30°C are a K_m of 0.38 μM and k_{cat} of 9.2 s⁻¹. In addition, it was shown that Rna1 from *S. pombe* can activate the hydrolysis in both human and *S. cerevisiae* Ran/Gsp1 with very similar observed rates of hydrolysis (Fig. 4a in Becker *et al.*⁴⁴).

Our conclusions are based on relative values between the wild-type Gsp1 and its point mutants. Although we report the absolute values of the kinetics parameters, when we compare the kinetics parameters with the results from genetic interaction profiling and AP-MS, we always use the relative parameters as compared to the wild type. Based on the sequence conservation and comparable kinetics described above, we expect the relative ordering of mutants to be similar as well. Importantly, we use the relative kinetic data to group our mutants into three classes. Even in the case of small quantitative differences caused by using the *S. pombe* instead of the *S. cerevisiae* Rna1 GAP, we make the assumption that these differences would not significantly affect this grouping.

Validity of the Michaelis-Menten formalism for GTPases

Michaelis-Menten formalisms have been used for multiple GTPases including Ran⁴⁵, Ras⁴⁶, or Rap⁴⁷. Historically there have been many attempts to formalize the conditions under which the Michaelis-Menten equation to describe enzyme kinetics are valid (as reviewed by Schnell⁴⁸). These conditions have converged on the steady-state approximation or more generally, on the reactant stationary assumption. The formal condition for steady-state approximation is that $t_{[ES]}$ (the time it takes for the steady-state levels of [ES] complex to accumulate) is substantially shorter than $t_{[S]}$ (the time where [S] changes significantly). The formal condition for reactant stationary assumption is that $[S] \approx [S_0]$ during initial build-up of [ES].

The formal condition for validity of the Michaelis-Menten equation can be expressed as:

$$\frac{[E_0]}{K_m + [S_0]} \ll \left(1 + \frac{K}{K_S}\right) \left(1 + \frac{[S_0]}{K_m}\right),$$

where $K = \frac{k_{cat}}{k_{on}}$ and $K_S = \frac{k_{off}}{k_{on}}$, and k_{off} and k_{on} are the rates of [ES] complex formation⁴⁹.

The measured dissociation constant, $K_S = \frac{k_{off}}{k_{on}}$, for the formation of the Ran:GDP:RCC1 complex from Ran:GDP and RCC1, where RCC1 is the human RanGEF, is 0.9 μM^{41} , which is approximately the same as the K_m value obtained for the GEF-mediated nucleotide exchange for both *S. cerevisiae* Gsp1 and human Ran. That means than $K \ll K_S$, which means the condition for validity of the Michaelis-Menten equation can be approximated as $\frac{[E_0]}{K_m + [S_0]} \ll \left(1 + \frac{[S_0]}{K_m}\right)$, and since in all of our GEF experiments both $[E_0] = 5-20 \text{ nM} \ll K_m$ and $[E_0] \ll [S_0]$, the conditions holds true for the entire range of $[S_0]$ values, both below and above the K_m .

As $\frac{K}{K_S}$ can also be expressed as $\frac{k_{cat}}{k_{off}}$, and the measured k_{off} of human Ran:GTP and RanGAP from *S. pombe* is estimated to be around 150 s^{-1} , while our measured k_{cat} values range from 1

to 10 s^{-1} , as above, $\frac{K}{K_S} \ll 1$ the assumption of steady-state holds true as long as $[E_0] \ll K_m$ and $[E_0] \ll [S_0]$, which is the case as we used 1-5 nM GAP in all of our experiments.

Supplementary Methods

Point mutations in genomic Gsp1 sequence

We identified all residues in Gsp1 that comprised the interfaces with Gsp1 binding partners for which co-complex crystal structures with Gsp1 were available (**Supplementary Fig. 1, Extended Data Fig. 1, Supplementary Table 1**). Residues comprising the interface *core*, the surface exposed *rim* around the core, and more buried *support* residues were defined based on per-residue relative solvent accessible surface area (rASA), as previously described²¹. rASA is compared to the empirical maximum solvent accessible surface area for each of the 20 amino acids⁵⁰. rASA values were calculated for the Gsp1 monomer (rASAmonomer) and for the complex (rASAComplex) using the bio3d R package⁵¹. The three types of interface residues were defined as: interface core if rASAmonomer > 25%, rASAComplex < 25% and ΔrASA (change upon complex formation) > 0; rim residues if rASAComplex > 25% and ΔrASA > 0; and support residues if rASAmonomer < 25% and ΔrASA > 0. All custom code for interface analysis from co-complex crystal structures is provided in the associated code repository at https://github.com/tinaperica/Gsp1_manuscript/tree/master/Scripts/complex_structure_analyses. We avoided Gsp1 residues that are within 5 Å of the nucleotide (GDP or GTP) in any of the structures or that are within the canonical small GTPase switch regions²² (P-loop, switch loop I, and switch loop II). We then mutated residues that are located in interface cores (defined as residues that bury more than 25% of their surface upon complex formation, as previously defined²¹, **Supplementary Table 2, Extended Data Fig. 1g**) into amino acid residues with a range of properties (differing in size, charge and polarity) and attempted to make stable and viable *S. cerevisiae* strains carrying a genomic Gsp1 point mutation coupled to nourseothricin (clonNAT / nourseothricin, Werner BioAgents GmbH, CAS 96736-11-7) resistance (**Supplementary Fig. 5**). The list of attempted mutants is provided in **Supplementary Table 3**. The genomic construct was designed to minimally disrupt the non-coding sequences known

at the time, including the 5' UTR and 3' UTR, as well as the putative regulatory elements in the downstream gene Sec72 (**Supplementary Fig. 5**). The *GSP1* genomic region was cloned into a pCR2.1-TOPO vector (Invitrogen) and point mutations in the *GSP1* coding sequence were introduced using the QuikChange™ Site-Directed Mutagenesis (Stratagene, La Jolla) protocol. *S. cerevisiae* strains containing mutant *GSP1* genes were regularly confirmed by sequencing the Gsp1 genomic region.

***S. cerevisiae* genetics and genetic interaction mapping**

***S. cerevisiae* transformation**

To generate MAT: α strains with Gsp1 point mutations the entire cassette was amplified by PCR using *S. cerevisiae* transformation forward and reverse primers, and *S. cerevisiae* was transformed into the starting SGA MAT: α his3D1; leu2D0; ura3D0; LYS2 β ; can1::STE2pr-SpHIS5 (SpHIS5 is the *S. pombe* HIS5 gene); lyp1D::STE3pr-LEU2 strain from²³ as described below.

Primers for amplifying the *GSP1* genomic region

| Primer name | Primer sequence |
|---|------------------------------------|
| <i>S. cerevisiae</i> Transformation FWD | GTATGATCAACTTTCTCACCTTTAAGTTGTTCG |
| <i>S. cerevisiae</i> Transformation REV | GATTGGAGAAACCAACCCAAATTTACACCAACAA |

DNA competent *S. cerevisiae* cells were made using a LiAc protocol. The final transformation mixture contained 10 mM LiAc (Lithium acetate dihydrate, 98%, extra pure, ACROS Organics™, CAS 6108-17-4), 50 µg ssDNA (UltraPure™ Salmon Sperm DNA Solution, Invitrogen, 15632011), 30 % sterile-filtered PEG 8000 (Poly(ethylene glycol), BioUltra, 8,000, Sigma-Aldrich, 89510-250G-F). A *S. cerevisiae* pellet of approximately 25 µl was mixed with 15 µl of linear DNA PCR product and 240 µl of the transformation mixture, and heat shocked at 42 °C for 40 minutes. Transformed cells were grown on YPD (20 g Bacto™ Peptone (CAT # 211820, BD Diagnostic Systems), 10 g Bacto™ Yeast Extract (CAT # 212720 BD), and 20 g Dextrose (CAT # D16-3, Fisher Chemicals) per 1-liter medium) + clonNAT plates and incubated at 30 °C for 3 to 6 days. Many colonies that appeared after 24-48 hours carried the clonNAT cassette but not the *GSP1* point mutation, or the 3xFLAG tag. Cells were therefore sparsely plated and plates were incubated for a longer period of time after which colonies of different sizes were picked and the mutant strains were confirmed by sequencing.

Epistatic mini-array profiling (E-MAP) of *Gsp1* point mutants

Genetic interactions of all viable *GSP1* point mutant (PM-GSP1-clonNAT) strains were identified by epistatic miniaarray profile (E-MAP) screens^{23,24} using a previously constructed array library of 1,536 KAN-marked (kanamycin) mutant strains assembled from the *S. cerevisiae* deletion collection²⁵ and the DAmP (decreased abundance by mRNA perturbation) strain collection²⁶, covering genes involved in a wide variety of cellular processes⁷. The E-MAP screen was conducted as previously described in Collins et al.²³, using the HT Colony Grid Analyzer Java program⁵ (http://sourceforge.net/project/showfiles.php?group_id=163953) and the E-MAP toolbox for MATLAB (http://sourceforge.net/project/showfiles.php?group_id=164376) to extract colony sizes of double mutant strains and a statistical scoring scheme to compute genetic interaction scores.

Genetic interaction scores represent the average of 3-5 independent replicate screens. Reproducibility was assessed as previously described⁵ by comparing individual scores to the average score for each mutant:gene pair, with the two values showing strong correlation across the dataset (Pearson correlation coefficient = 0.83, **Supplementary Fig. 6**).

Hierarchical clustering of E-MAP genetic interaction data

All E-MAP library DAmP strains as well as library strains showing poor reproducibility were discarded, leaving 1444 out of the original 1536 library genes. Averaged S-scores of genetic interactions between wild-type and point mutant Gsp1 and the 1444 *S. cerevisiae* genes are provided in **Source File 1**. Hierarchical clustering on the GI profiles was performed using the average linkage method and the pairwise Pearson correlation coefficient as a distance metric. To identify clusters of functionally related library genes, the hierarchical clustering tree was cut to produce 1200 clusters, resulting in 43 clusters with 3 or more members. Biological function descriptions for genes in these clusters were extracted from the *Saccharomyces* Genome Database (SGD)²⁷. Clusters of genes representing common functions (complexes, pathways or biological functions) were selected by manual inspection and represented in the main text **Fig. 1c** and **Extended Data Fig. 4b**. All custom code for E-MAP analysis is provided in https://github.com/tinaperica/Gsp1_manuscript/tree/master/Scripts/E-MAP. Clustered heatmaps were produced using the ComplexHeatmap package⁵².

Scaling of published genetic interaction data to the E-MAP format

To enable comparison of *GSP1* point mutant GI profiles to GI profiles of other *S. cerevisiae* genes, published Synthetic Gene Array (SGA) genetic interaction data¹⁴ from CellMap.org⁵³ were scaled to the E-MAP format using a published non-linear scaling method⁵⁴. First, 75,314 genetic interaction pairs present in both the SGA and a previously described E-MAP dataset

used to study chromatin biology²⁶ were ordered by genetic interaction score and partitioned into 500 equally sized bins separately for each dataset. Bin size (150 pairs per bin) was chosen to provide enough bins for fitting the scaling spline (described below) while still maintaining a large number of pairs per bin such that the mean could be used as a high confidence estimate of the score values in each bin. Scaling factors were computed that scaled the mean of each SGA bin to match the mean of the corresponding E-MAP bin. A non-linear univariate spline was fit through the scaling factors, providing a scaling function that was subsequently applied to each SGA score. The distribution of scores of shared interactions between the scaled SGA and the E-MAP chromatin library was similar to that between replicates in the E-MAP chromatin library, matching what was seen in the previously published scaling of SGA data to E-MAP format⁵⁴ (**Supplementary Fig. 10**). The SGA genetic interaction scores are taken from CellMap.org⁵³. The scaling code is provided in

https://github.com/tinaperica/Gsp1_manuscript/tree/master/Scripts/SGA_Scaling.

Significance of genetic interactions

The S-score metric used in scoring genetic interactions measured by the E-MAP method has been previously characterized in terms of confidence that any given averaged S-score represents a significant interaction⁵. We fit a spline to data points from Fig. 4c from Collins et al⁵, allowing us to provide an approximate confidence estimate for each of our measured *GSP1* and scaled *S. cerevisiae* SGA genetic interaction scores. The SGA dataset¹⁴ is accompanied by p-values as well as its own recommendations for a threshold at which individual interactions are considered significant. We plotted the SGA score scaled to E-MAP format vs. the associated p-value (negative log-transformed, **Supplementary Fig. 2a**) and found the distribution to have a similar shape to the confidence function for S-scores (**Supplementary Fig. 2b**). For example, a 95% confidence threshold is associated with E-MAP S-scores less

than -4 or greater than 5, while the median p-value of scaled SGA scores is less than 0.05 for scores less than -5 or greater than 3. We ultimately elected to use a significance cutoff of absolute S-score greater than 3. This threshold corresponds to an estimated confidence value of 0.83 for S-scores less than -3 and 0.65 for S-scores greater than 3. We compared these values to the intermediate significance threshold recommended for the SGA data from Ref.¹⁴, which was p-value < 0.05 and absolute SGA score > 0.08. After scaling to E-MAP format, this threshold corresponds to scaled S-scores less than -2.97 or greater than 2.25, below our chosen threshold of -3 and 3.

GI profile correlation measurements

Of the 1444 library genes in the *GSP1* point mutant GI profile map, 1129 were present in the SGA dataset from Ref.¹⁴. Pairwise Pearson correlation coefficients were computed between all *GSP1* point mutants and SGA gene profiles, and all profiles trimmed to include only genetic interaction measurements with the 1129 shared library genes. Due to the relative sparsity of GI profiles, pairwise comparisons are dominated by high numbers of non-significant interactions. Accordingly, we did not consider correlations with *GSP1* point mutants or SGA gene profiles that did not have significant genetic interactions (absolute scaled S-score greater than 3, see above) with at least 10 of the 1129 library genes. This requirement removed all weak Gsp1 point mutants and one strong mutant (R108A) from the correlation analysis (as they had at most nine genetic interactions with absolute score greater than 3), leaving 22 strong mutants and 3370 *S. cerevisiae* SGA alleles to be included in the correlation analysis. All Pearson correlations and their p-values between Gsp1 mutants and *S. cerevisiae* genes, including all correlations that did not pass our significance filtering procedures, are provided in **Source File 2**. The subset of Pearson correlations between Gsp1 point mutants and Gsp1 partners with

available co-complex X-ray crystal structures, used to make the point plots in **Fig. 1e** and **Extended Data Fig. 4c,d**, are also available in **Supplementary Table 4**.

Statistical significance of correlations was computed using both two-sided and one-sided (positive) t-tests adjusted for multiple hypothesis testing using both the Bonferroni method and the FDR method, which controls the false discovery rate²⁸. All p-values reported in the text and figures are one-sided (positive) and corrected by the FDR method, unless otherwise stated.

The FDR method of p-value correction has been shown to account for the positive dependency between test statistics, such as those arising from the underlying functional similarities between *S. cerevisiae* alleles²⁹. Custom code for GI profile correlation calculations and filtering is provided in the accompanying repository

https://github.com/tinaperica/Gsp1_manuscript/tree/master/Scripts/E-MAP/correlations.

Significance testing was used to filter out *S. cerevisiae* gene SGA profiles that did not show a significant correlation (one-sided positive, Bonferroni-adjusted) with the GI profiles of at least two *GSP1* point mutants. In total, 276 *S. cerevisiae* alleles from the SGA had a significant GI profile correlation (one-sided positive, Bonferroni-adjusted) with at least two *GSP1* point mutants and were therefore included in the correlation analysis shown in **Fig. 4a**. We required alleles to correlate with at least two mutants because the goal of this analysis was to group mutants by similarity, and an allele that only significantly correlated with one mutant is uninformative for this task. After this filtering step, the one-sided p-values were used to populate a matrix of 22 mutants vs. 276 alleles, and hierarchical clustering was performed using Ward's method. We used Ward's method rather than the average linkage criterion as we found the latter resulted in a wide variety of group sizes due to a few sparsely populated outliers. Using Ward's methods resulted in rounder clusters, allowing us to identify meaningful functional groups of mutants and alleles. Pearson correlation between correlation vectors was

used as a distance metric for the mutant (row) clustering, while Euclidean distance was selected for the gene (column) clustering, due to the column vectors being relatively short (22 mutants per column vs. 276 alleles per row) and thus sensitive to outliers when clustered using Pearson correlations as the distance metric (for additional analysis of E-MAP statistics and clustering see **Supplementary Discussion**).

For the gene set analysis we decreased the stringency of inclusion of *S. cerevisiae* SGA genes to include all alleles with a significant GI profile correlation (one-sided positive, Bonferroni-adjusted) with one or more Gsp1 mutants, which added another 201 alleles, resulting in 477 alleles. We made the gene sets larger to increase our confidence in connecting the patterns of correlations between *S. cerevisiae* genes and Gsp1 mutants to the GTPase cycle parameters represented in **Fig. 4b, d**. Indeed, while *S. cerevisiae* genes that only correlate significantly with one mutant are not informative for grouping mutants, they are informative for annotating the functional effects of individual mutants. Manually curated gene sets of *S. cerevisiae* genes with significant correlations with Gsp1 mutants are provided in **Source File 4**.

Protein expression levels by Western Blot

S. cerevisiae strains were grown at 30°C in YPD medium (20 g Bacto™ Peptone (CAT # 211820, BD Diagnostic Systems), 10 g Bacto™ Yeast Extract (CAT # 212720 BD), and 20 g Dextrose (CAT # D16-3, Fisher Chemicals) per 1 L medium) for 1.5 - 2 hours until OD₆₀₀ reached 0.3. Cell culture aliquots of 1 ml were centrifuged for 3 minutes at ~ 21,000 x g and resuspended in 30 µl of phosphate buffered saline (137 mM NaCl, 2.7 mM KCl, 10 mM Na₂HPO₄, 1.8 mM KH₂PO₄, pH = 7.4) and 10 µl of SDS-PAGE Sample Buffer (CAT # 161-0747, BioRad), to a final SDS concentration of 1%, and ~ 2mM beta-mercaptoethanol. Lysates were run (3 µl for most, and 6 µl for slow growing mutants with lower OD₆₀₀) on Stain-Free gels (4-20%, CAT #4568096, BioRad, Tris/Glycine SDS Buffer (CAT #161-0732, BioRad)).

After electrophoresis, the gel was scanned for total protein quantification and the proteins were subsequently transferred to an Immobilon-FL PVDF membrane (CAT #IPF00010, EMD Millipore). The membrane was probed with Rabbit anti-RAN (CAT # PA 1-5783, ThermoFisher Scientific) primary, and Goat anti-Rabbit-IgG(H+L)-HRP (CAT #31460, Thermo Fisher) secondary antibodies. The membrane was developed using Super Signal West Femto substrate (CAT # 34096, Thermo Fisher), and scanned and analyzed with Image Lab software on a ChemiDoc MP (BioRad). Each blot had at least one wild-type (WT-GSP1-clonNAT) and at least one MAT: α strain control. The total protein levels (TP^{MUT}) for each Gsp1 point mutant lane were then normalized to the wild-type (WT-GSP1-clonNAT) lane of the corresponding blot (TP^{WT}), providing an adjustment value to account for differences in loading between lanes ($a^{MUT} = \frac{TP^{MUT}}{TP^{WT}}$). To compute the relative expression of a Gsp1 point mutant, the density (D^{MUT}) of the Western blot bands corresponding to the Gsp1 point mutant was divided by the total protein adjustment and finally normalized against the same value for the wild-type Gsp1, i.e. $rel.\ expression^{MUT} = \frac{D^{MUT}/a^{MUT}}{D^{WT}/a^{WT}}$. Note that for blots with a single WT lane, $a^{WT} = 1$. For blots with more than one WT lane included, a^{WT} was computed for each WT lane by normalizing to the average TP across all WT lanes, and the average adjusted WT density (D^{WT}/a^{WT}) across all WT lanes was used for computing the relative expression of point mutants. An example Western blot is provided in **Supplementary Fig. 11**, and the final protein expression level data for all mutants are shown in **Extended Data Fig. 2**.

Physical interaction mapping using affinity purification mass spectrometry (AP-MS)

S. cerevisiae cell lysate preparation

When choosing mutants for AP-MS we sought to cover all Gsp1 sequence positions where mutations had strong GI profiles (**Extended Data Fig. 4a**), as well as several ‘weak’ mutants. We observed that tagging the endogenous Gsp1 with either an amino-terminal or a carboxy-terminal FLAG tag affects the *S. cerevisiae* growth in culture. We therefore attempted to make each of the mutants intended for AP-MS experiments with both tags, and where both tags were viable, we obtained the AP-MS data for both. We could not make a FLAG-tagged R108Q mutant for AP-MS. *S. cerevisiae* strains for AP-MS were grown in YAPD medium (120 mg adenine hemisulfate salt (CAT # A9126, SIGMA), 10 g Bacto yeast extract (CAT # BD 212720), 20 g Bacto peptone (CAT # BD 211820), 20 g dextrose (D-glucose D16-3 Fisher Chemicals) per 1 L of medium). Each strain was grown at 30°C for 12 to 24 h to OD₆₀₀ of 1-1.5. The cells were harvested by centrifugation at 3000 RCF for 3 minutes and the pellet was washed in 50 ml of ice-cold ddH₂O, followed by a wash in 50 ml of 2x lysis buffer (200 mM HEPES pH 7.5, 200 mM KCl, 2 mM MgCl₂, 30 µM GTP (Guanosine 5'-triphosphate sodium salt hydrate, CAT #G8877, Sigma-Aldrich), 1 mM Dithiothreitol (Promega V3151), 0.1% IGEPAL CA-630 (CAT # I8896, Sigma-Aldrich), and 10% glycerol). Each pellet of approximately 500 µl was then resuspended in 500 µl of 2X lysis buffer supplemented with protease inhibitors without EDTA (cComplete, Mini, EDTA-free Protease Inhibitor Cocktail, CAT # 11836170001, Roche) and dripped through a syringe into liquid nitrogen. The frozen *S. cerevisiae* cell pellets were lysed in liquid nitrogen with a SPEX™ SamplePrep 6870 Freezer/Mill™.

FLAG immunoprecipitation

FLAG immunoprecipitations were performed as previously described^{30,31}. Details are as follows. For FLAG immunoprecipitations, frozen samples were initially kept at room temperature for 5 minutes and then placed on ice or at 4°C in all subsequent steps, unless indicated otherwise. Following the addition of 1.5 – 3.0 ml Suspension Buffer (0.1 M HEPES pH 7.5, 0.1 M KCl, 1 mM MgCl₂, 15 µM GTP, and 0.5 mM Dithiothreitol) supplemented with cComplete mini EDTA-free protease and PhosSTOP phosphatase inhibitor cocktails (Roche), samples were incubated on a rotator for at least 10 minutes and then adjusted to 6.0 ml total volume with additional Suspension Buffer supplemented with inhibitors before centrifugation at 18,000 rpm for 10 minutes. Anti-FLAG M2 Affinity Gel beads (50 µl slurry; Sigma-Aldrich) were washed twice with 1.0 ml Suspension Buffer. After reserving 50 µl, the remaining supernatant and anti-FLAG M2 Affinity Gel beads were combined and incubated for >= 2 hours on a tube rotator. Beads were then collected by centrifugation at 300 rpm for 5 minutes and washed three times. For each wash step, beads were alternately suspended in 1.0 ml Suspension Buffer and collected by centrifugation at 2,000 rpm for 5 minutes. After removing residual wash buffer, proteins were eluted in 42 µl 0.1 mg/ml 3xFLAG peptide, 0.05% RapiGest SF Surfactant (Waters Corporation) in Suspension Buffer by gently agitating beads on a vortex mixer at room temperature for 30 minutes. Immunoprecipitated proteins (~4 µl) were resolved on 4-20% Criterion Tris-HCl Precast gels (BioRad) and visualized by silver stain (Pierce Silver Stain Kit; Thermo Scientific) (**Supplementary Fig. 12**) before submitting 10 µl of each sample for mass spectrometry. At least three independent biological replicates were performed for each FLAG-tagged protein and the untagged negative control.

Liquid chromatography with tandem mass spectrometry (LC-MS/MS) analysis

To prepare samples for LC-MS/MS analysis, immunoprecipitated protein (10 µl) was denatured and reduced in 2 M urea, 10 mM NH₄HCO₃, and 2 mM Dithiothreitol for 30 minutes at 60°C with constant shaking, alkylated in the dark with 2 mM iodoacetamide for 45 minutes at room temperature and digested overnight at 37°C with 80 ng trypsin (Promega). Following digestion, peptides were acidified with formic acid and desalted using C18 ZipTips (Millipore) according to the manufacturer's specifications. Samples were re-suspended in 4% formic acid, 2% acetonitrile solution, and separated by a 75-minute reversed-phase gradient over a nanoflow C18 column (Dr. Maisch). Peptides were directly injected into a Q-Exactive Plus mass spectrometer (Thermo), with all MS1 and MS2 spectra collected in the orbitrap. Raw MS data were searched against the *S. cerevisiae* proteome (SGD sequences downloaded January 13, 2015) using the default settings in MaxQuant (version 1.5.7.4), with a match-between-runs enabled^{32,33}. Peptides and proteins were filtered to 1% false discovery rate in MaxQuant, and identified proteins were then subjected to protein-protein interaction scoring using SAINTexpress³⁴. Protein were filtered to only those representing high confidence protein-protein interactions (Bayesian false discovery rate from SAINT (SAINT BFDR) < 0.05). Protein abundance values for this filtered list were then subjected to equalized median normalization, label free quantification and statistical analysis were performed using MSstats³⁵, separately for data from amino- or carboxy-terminally tagged baits. Fold change in abundance of preys for 3xFLAG-tagged Gsp1 point mutants was always calculated compared to the wild-type Gsp1 with the corresponding tag. All AP-MS data are available from the PRIDE repository under the PXD016338 identifier. Fold change values between prey abundance between the mutant and wild-type Gsp1 and the corresponding FDR adjusted p-values are provided in **Source File 3**. The intersection of all prey proteins identified at least once with both the amino- or carboxy-terminal 3xFLAG tag, and their interquartile ranges

(IQR) of log₂-transformed fold change values across all the Gsp1 mutants, are provided in **Supplementary Table 5**. Quality of data and reproducibility between replicates was assessed based on correlations of protein abundance between replicates (**Supplementary Figs. 7, 8**).

Biochemical and biophysical assays

Protein purifications

All proteins were expressed from a pET-28 a (+) vector with a N-terminal 6xHis tag in *E. coli* strain BL21 (DE3) in the presence of 50 mg/L Kanamycin for 2xYT medium, and 100 mg/L of Kanamycin for autoinduction EZ medium. GEF (Srm1 from *S. cerevisiae*, (Uniprot P21827)) was purified as Δ1-27Srm1 and GAP (Rna1 from *S. pombe*, Uniprot P41391) as a full-length protein (for use of *S. pombe* Rna1 see **Supplementary Discussion**). ScΔ1-27Srm1 and SpRna1 were expressed in 2xYT medium (10 g NaCl, 10 g yeast extract (BD Bacto™ Yeast Extract #212720), 16 g tryptone (Fisher, BP1421) per 1 L of medium) overnight at 25 °C upon addition of 300 μmol/L Isopropyl-β-D-thiogalactoside (IPTG). Gsp1 variants were expressed by autoinduction for 60 hours at 20°C³⁶. The autoinduction medium consisted of ZY medium (10 g/L tryptone, 5 g/L yeast extract) supplemented with the following stock mixtures: 20xNPS (1M Na₂HPO₄, 1M KH₂PO₄, and 0.5 M (NH₄)₂SO₄), 50x 5052 (25% glycerol, 2.5% glucose, and 10% α-lactose monohydrate), 1000x trace metal mixture (50 mM FeCl₃, 20 mM CaCl₂, 10 mM each of MnCl₂ and ZnSO₄, and 2 mM each of CoCl₂, CuCl₂, NiCl₂, Na₂MoO₄, Na₂SeO₃, and H₃BO₃ in ~60 mM HCl). Cells were lysed in 50 mM Tris pH 7.5, 500 mM NaCl, 10 mM imidazole, and 2 mM β-mercaptoethanol using a microfluidizer from Microfluidics. For Gsp1 purifications, the lysis buffer was also supplemented with 10 mM MgCl₂. The His-tagged proteins were purified on Ni-NTA resin (Thermo Scientific #88222) and washed into a

buffer containing 50 mM Tris (pH 7.5) and 100 mM NaCl, with 5 mM MgCl₂ for Gsp1 proteins. The N-terminal His-tag was digested at room temperature overnight using up to 12 NIH Units per mL of bovine thrombin (Sigma-Aldrich T4648-10KU). Proteins were then purified using size exclusion chromatography (HiLoad 26/600 Superdex 200 pg column from GE Healthcare), and purity was confirmed to be at least 90% by SDS polyacrylamide gel electrophoresis. Samples were concentrated on 10 kDa spin filter columns (Amicon Catalog # UFC901024) into storage buffer (50 mM Tris pH 7.5, 150 mM NaCl, 1 mM Dithiothreitol). Storage buffer for Gsp1 proteins was supplemented with 5 mM MgCl₂. Protein concentrations were confirmed by measuring at 10-50x dilution using a Nanodrop (ThermoScientific). The extinction coefficient at 280 nm used for nucleotide (GDP or GTP) bound Gsp1 was 37675 M⁻¹ cm⁻¹, as described in⁵⁵. The ratio of absorbance at 260 nm and 280 nm for purified Gsp1 bound to GDP was 0.76. Extinction coefficients for other proteins were estimated based on their primary protein sequence using the ProtParam tool (<https://web.expasy.org/protparam/>). Concentrated proteins were flash-frozen and stored at -80 °C.

In our hands every attempt to purify the *S. cerevisiae* homologue of GAP (Rna1, Uniprot P11745) from *E. coli* yielded a protein that eluted in the void volume on the Sephadex 200 size exclusion column, indicating that the protein is forming soluble higher-order oligomers. We were, however, successful in purifying the *S. pombe* homologue of GAP (Rna1, Uniprot P41391) as a monomer of high purity as described above, and we used the purified *S. pombe* homolog of Rna1 in all of our GTP hydrolysis kinetic experiments. Although we cannot exclude slight differences between the kinetic parameters of *S. pombe* and *S. cerevisiae* Rna1, we do not believe such differences would significantly affect our conclusions for two main reasons: First, residues in the interface with Gsp1 are highly conserved between *S. pombe* and *S. cerevisiae* GAP Rna1, suggesting that mechanism of catalysis and kinetic parameters are also likely to be similar. *S. pombe* and *S. cerevisiae* Rna1 proteins have an overall 39%

sequence identity and 53% sequence similarity. Importantly, all but one interface core residues are identical in sequence between *S. cerevisiae* and *S. pombe* homologues (**Supplementary Fig. 9**). The X-ray crystal structure of Ran GTPase and its GAP used in our analyses is a co-complex structure of the *S. pombe* homolog of Rna1 (PDB: 15kd), human Ran, and human RanBP1 (**Supplementary Table 1**). Second, we rely only on the *relative differences* between GAP kinetic parameters of different Gsp1 mutants to group our mutants into three classes. Even in the case of differences between the absolute kinetic parameters between the *S. pombe* and *S. cerevisiae* GAP Rna1, the order of mutants is less likely to be different, and even in the case of some differences, we expect the grouping to be robust to these changes (see **Supplementary Discussion** for more detail).

Circular dichroism (CD) spectroscopy of protein thermostability

Samples for CD analysis were prepared at approximately 2 μ M Gsp1 in 2 mM HEPES pH 7.5, 5 mM NaCl, 200 μ M MgCl₂, and 50 μ M Dithiothreitol. CD spectra were recorded at 25 °C using 2 mm cuvettes (Starna, 21-Q-2) in a JASCO J-710 CD-spectrometer (Serial #9079119). The bandwidth was 2 nm, rate of scanning 20 nm/min, data pitch 0.2 nm, and response time 8 s. Each CD spectrum represents the accumulation of 5 scans. Buffer spectra were subtracted from the sample spectra using the Spectra Manager software Version 1.53.01 from JASCO Corporation. Temperature melts were performed from 25°C - 95°C, monitoring at 210 nm, using a data pitch of 0.5°C and a temperature slope of 1°C per minute. As all thermal melts of wild-type and mutant Gsp1 proteins were irreversible, only apparent T_m was estimated (**Supplementary Fig. 13**) and is reported in **Supplementary Table 9**.

GTP loading of Gsp1

Gsp1 variants for GTPase assays as well as for ^{31}P NMR spectroscopy were first loaded with GTP by incubation in the presence of 20-fold excess GTP (Guanosine 5'-Triphosphate, Disodium Salt, CAT # 371701, Calbiochem) in 50 mM Tris HCl pH 7.5, 100 mM NaCl, 5 mM MgCl₂. Exchange of GDP for GTP was initiated by the addition of 10 mM EDTA. Reactions were incubated for 3 hours at 4°C and stopped by addition of 1 M MgCl₂ to a final concentration of 20 mM MgCl₂ to quench the EDTA. GTP-loaded protein was buffer exchanged into either NMR buffer or the GTPase assay buffer using NAP-5 Sephadex G-25 DNA Grade columns (GE Healthcare # 17085301). We were unable to obtain sufficient material for some mutants (H141E/I, Y148I), for which we collected AP-MS data, since these mutants precipitated during the nucleotide exchange process at the high concentrations required for ^{31}P NMR, possibly because of the limited stability of nucleotide-free Ran/Gsp1 generated during exchange, as noted previously⁴⁵.

Reverse phase high performance liquid chromatography (HPLC)

Analysis of bound nucleotide was performed using reverse-phase chromatography as previously described⁵⁵ using a C18 column (HAISIL TS Targa C18, particle size 5 μm , pore size 120 Å, dimensions 150 x 4.6 mm, Higgins Analytical # TS-1546-C185). The column was preceded by a precolumn filter (The Nest Group, Inc, Part # UA318, requires 0.5 μm frits, Part # UA102) and a C18 guard column (HAICart SS Cartridge Column, HAISIL Targa C18, 3.2x20 mm, 5 μm , 120 Å Higgins Analytical # TF-0232-C185, requires a Guard Holder Kit, Higgins Analytical # HK-GUARD-FF). To prepare the nucleotide for analysis, a Gsp1 sample was first diluted to a concentration of 25-30 μM and a volume of 40 μl . The protein was denatured by addition of 2.5 μl of 10% perchloric acid (HClO₄). The pH was raised by addition of 1.75 μl 4 M sodium acetate (CH₃COONa) pH 4.0. The nucleotide was separated from the

precipitated protein before application to the column by spinning at 20,000 x g for 20 minutes. 30 µl of supernatant was withdrawn and mixed 1:1 with reverse-phase buffer (10 mM tetra-n-butylammonium bromide, 100 mM KH₂PO₄ / K₂HPO₄, pH 6.5, 0.2 mM NaN₃). 20 µl of sample was injected onto the equilibrated column and run isocratically in 92.5% reverse-phase buffer, 7.5% acetonitrile at a flow rate of 1 ml/min for 35 min (~20 column volumes). Nucleotide retention was measured by monitoring absorbance at both 254 nm and 280 nm. Example HPLC reverse phase chromatogram of GTP-loaded wild-type Gsp1 is shown in **Supplementary Fig. 14.**

NMR Spectroscopy

Gsp1 samples for ³¹P NMR spectroscopy were first loaded with GTP as described above, and buffer exchanged into NMR Buffer (D₂O with 50 mM Tris-HCl pH 7.4, 5 mM MgCl₂, 2 mM Dithiothreitol). Final sample concentrations were between 250 µM and 2 mM, and 400 µl of sample were loaded into 5 mm Shigemi advanced microtubes matched to D₂O (BMS-005TB; Shigemi Co. Ltd, Tokyo, Japan.). ³¹P NMR experiments were performed on a Bruker Avance III 600 MHz NMR spectrometer with a 5 mm BBFO Z-gradient Probe. Spectra were acquired and processed with the Bruker TopSpin software (version 4.0.3). Indirect chemical shift referencing for ³¹P to DSS (2 mM Sucrose, 0.5 mM DSS, 2 mM NaN₃ in 90% H₂O + 10% D₂O; water-suppression standard) was done using the IUPAC-IUB recommended ratios³⁷. Spectra were recorded at 25°C using the pulse and acquire program zg (TopSpin 3.6.0), with an acquisition time of 280 milliseconds, a recycle delay of 3.84 seconds, and a 65° hard pulse. *4,096 complex points were acquired over the course of 4,096 scans and a total acquisition time of 4.75 hours. Spectra were zero-filled once and multiplied with an exponential window function (EM) with a line-broadening of 6 Hz (LB = 6) prior to Fourier transformation. Peaks were integrated using the auto-integrate function in TopSpin 4.0.7, and peak areas were

referenced to the bound GTP- β peak of each spectrum. The peak at approximately -7 ppm is defined as γ 1 and the peak at approximately -8 ppm is defined as γ 2. The percent of γ phosphate in γ 2 is defined as a ratio of areas under the curve between the γ 2 and the sum of the γ 1 and γ 2 peaks.

Kinetic measurements of GTP hydrolysis.

Kinetic parameters of the GTP hydrolysis reaction were determined using a protocol similar to one previously described³⁸. Gsp1 samples for GTP hydrolysis kinetic assays were first loaded with GTP as described above. GTP hydrolysis was monitored by measuring fluorescence of the *E. coli* phosphate-binding protein labeled with 7-Diethylamino-3-[N-(2-maleimidooethyl)carbamoyl]coumarin (MDCC) (phosphate sensor, CAT # PV4406, Thermo Fisher) upon binding of the free phosphate GTP hydrolysis product (excitation at 425 nm, emission at 457 nm). All experiments were performed in GTPase assay buffer (40 mM HEPES pH 7.5, 100 mM NaCl, 4 mM MgCl₂, 1 mM Dithiothreitol) at 30°C in 100 μ l reaction volume on a Synergy H1 plate reader from BioTek, using Corning 3881 96-well half-area clear-bottom non-binding surface plates. The phosphate sensor at 20 μ M and 50 μ M concentrations was calibrated with a range of concentrations of K₂HPO₄ using only the data in the linear range to obtain a conversion factor between fluorescence and phosphate concentration. For each individual GAP-mediated GTP hydrolysis experiment, a control experiment with the same concentration of GTP-loaded Gsp1 and the same concentration of sensor, but without added GAP, was run in parallel. The first 100 s of these data were used to determine the baseline fluorescence, and the rest of the data were linearly fit to estimate intrinsic GTP hydrolysis rate (**Supplementary Table 8**). Although we do estimate the intrinsic hydrolysis rates from the background data, the estimate is only approximate, as well as 10⁵ to 10⁶ lower than the rate of GAP-mediated GTP hydrolysis, which is why we do not use intrinsic hydrolysis rates when

fitting the GAP-mediated hydrolysis data. The affinity of Rna1 for GDP-bound Ran is negligible (K_d of 100 μM for Ran:GDP⁵⁶, which is \sim 250-fold weaker than the estimated K_m for GAP-mediated GTP hydrolysis) and was not taken into account when fitting the data.

As the estimated K_m for the GAP-mediated hydrolysis for many of the Gsp1 variants was low (in the 0.1-0.4 μM range, resulting in difficulties to reliably measure hydrolysis at low substrate concentrations), we sought to estimate the kinetic parameters (k_{cat} and K_m) by directly analysing the full reaction progress curve with an analytical solution of the integrated Michaelis-Menten equation (see section below for details).

Estimating the k_{cat} and K_m parameters of GAP-mediated hydrolysis using an accurate solution to the integrated Michaelis-Menten equation.

Others (e.g. Goudar *et al*³⁹) have shown that both k_{cat} and K_m can be estimated with reasonable accuracy/precision from a single time-course with *initial* $[S] > K_m$ by directly analyzing the *full* reaction progress curve with an analytical solution of the *integrated* Michaelis-Menten equation based on the Lambert ω function. This analysis is possible because the full reaction progress curve is characterized by an initial linear phase for $[S] > K_m$, a final exponential phase for $[S]$, and a transition phase for $[S] \sim K_m$. Whereas k_{cat} is sensitive to the slope of the initial linear phase (i.e. the initial velocity), K_m is sensitive to the shape of the progress curve, which will have an extended linear phase if $K_m \ll$ initial $[S]$ or no linear phase if $K_m \gg$ initial $[S]$. Use of the integrated Michaelis-Menten analysis requires the experiment to be set up with the following conditions: (i) $[\text{Gsp1:GTP}_0] > K_m$, (ii) $[\text{GAP}_0] \lll [\text{Gsp1:GTP}_0]$, and (iii) the reaction time course $F(t)$ is measured to completion (i.e. until it approaches equilibrium). Our experiments were all set up to fulfill those conditions, which means that the $F(t)$ sampled a concentration range from $[\text{Gsp1:GTP}]$ (at $t = 0$) $> K_m$ to $[\text{Gsp1:GTP}]$ (at $t = \text{final time}$) $\ll K_m$. The entire $F(t)$ can then be directly analyzed by a non-linear fit with the analytical solution for

the integrated Michaelis-Menten equation. As the initial linear phase of the time course is well measured, k_{cat} can be well determined. As the exponential phase and transition region of the time course are also well measured, the maximum likelihood value of K_m can also be determined.

Specifically, each time course was fitted to an integrated Michaelis-Menten equation:

$$\text{fluorescence} = B + [E]_t(C_i + (C_f - C_i)(1 - K_m * \frac{\omega}{[S]_0})),$$

where $[E]_t$ is the total enzyme (GAP) concentration, C_i is the initial fluorescence, C_f is the final fluorescence, $[S]_0$ is the initial concentration of the substrate (GTP loaded Gsp1), and B is the baseline slope in fluorescence per second. Exact concentration of loaded Gsp1:GTP $[S]_0$ was estimated based on the plateau fluorescence and the sensor calibration parameters to convert the fluorescence to free phosphate concentration. The ω parameter was solved by using the Lambert ω algorithm, as previously described³⁹, where

$$\omega = \text{Lambert omega}(\frac{[S]_0}{K_m} e^{\frac{[S]_0 - k_{cat}[E]t*time}{K_m}}).$$

The curves were fit with the custom-made software DELA⁴⁰. Examples of full reaction progress curves and their integrated Michaelis-Menten fits are shown in **Supplementary Fig. 3**.

We confirmed that the kinetic value parameters we obtained for wild-type Gsp1 using the phosphate sensor and integrated Michaelis-Menten equation were similar to those estimated using intrinsic tryptophan fluorescence⁴¹. Their values were a K_m of 0.45 μM and k_{cat} of 2.1 s^{-1} at 25°C for mammalian Ran hydrolysis activated by *S. pombe* GAP, while our values for wild type *S. cerevisiae* Gsp1 and *S. pombe* GAP at 30°C are K_m of 0.38 μM and k_{cat} of 9.2 s^{-1} .

For most mutants a concentration of 1 nM GAP (SpRna1, Rna1 from *S. pombe*) was used. In order to run the time courses to completion, for mutants with low k_{cat}/K_m enzyme concentrations of 2-5 nM were used. Initially we collected time course data for all Gsp1 variants at approximately 8 μ M concentration of loaded Gsp1:GTP with 1 nM GAP and 20 μ M phosphate sensor. If the estimated K_m was higher than 1 μ M, we repeated the time course kinetic experiments with higher concentration of Gsp1:GTP of approximately tenfold above the K_m .

To quantify the accuracy of parameter (k_{cat} , K_m) estimation for GAP-mediated GTP-hydrolysis by the integrated Michaelis-Menten approach over a range of kinetic parameters and substrate concentrations [Gsp1:GTP] we simulated data covering the range of parameters estimated for all of our Gsp1 point mutants, and estimated the accuracy of parameters determined given the Gaussian noise similar to our experimental data. The largest standard deviations were 3%, 17%, and 18% for k_{cat} , K_m , and k_{cat}/K_m , respectively (**Supplementary Fig. 15**). In addition, we analysed how the χ^2 statistic changed as the Michaelis-Menten parameters were systematically varied around the estimated maximum likelihood values (**Supplementary Fig. 16**). For these analyses, the k_{cat} or K_m values were independently fixed and incremented while the remaining parameters were fit to generate χ^2 surfaces for one degree of freedom. Confidence intervals (CIs) for which χ^2 increased by 4.0 compared to the maximum likelihood minimum were estimated by linear interpolation after iterative bisection. A χ^2 increase of 4.0 corresponds to the 95% confidence limit for a normal distribution. The k_{cat}/K_m ratio and corresponding χ^2 values were derived from the analyses with systematic variation of either k_{cat} or K_m . CIs for k_{cat}/K_m were estimated by linear interpolation without iterative bisection. The χ^2 surfaces approach a parabolic shape with a well-defined minimum at the maximum likelihood value. The CIs are further consistent with the parameter ranges obtained from the simulations. Thus,

both the simulations and χ^2 surfaces indicate that k_{cat} and K_m are estimated with reasonable accuracy over the range of parameter values and experimental conditions used in this study.

The Michaelis Menten k_{cat} and K_m parameters and their standard deviations were calculated from at least three technical replicates from two or more independently GTP-loaded Gsp1 samples (**Supplementary Table 6**). For more details on the kinetic analysis see **Supplementary Discussion**.

Kinetic measurements of Srm1 mediated nucleotide exchange.

Kinetic parameters of GEF mediated nucleotide exchange were determined using a fluorescence resonance energy transfer (FRET) based protocol⁴¹. Each Gsp1 variant was purified as a Gsp1:GDP complex, as confirmed by reverse phase chromatography. Nucleotide exchange from GDP to mant-GTP (2'-(or-3')-O-(N-Methylanthraniloyl) Guanosine 5'-Triphosphate, CAT # NU-206L, Jena Biosciences) was monitored by measuring a decrease in intrinsic Gsp1 tryptophan fluorescence (295 nm excitation, 335 nm detection) due to FRET upon binding of the mant group. Each time course was measured in GEF assay buffer (40 mM HEPES pH 7.5, 100 mM NaCl, 4 mM MgCl₂, 1 mM Dithiothreitol) with excess of mant-GTP. The affinity of Ran/Gsp1 is estimated to be 7-11-fold lower for GTP than for GDP⁴⁵, and for most variants of Gsp1 we measured time courses at Gsp1:GDP concentrations ranging from 0.25 to 12 μ M with an excess mant-GTP concentration of 200 μ M. For Gsp1 variants with high K_m values that had to be measured at concentrations of up to 200 μ M we used an excess of 1000 μ M mant-GTP. In addition, we fit the data using a combination of fits following the approach of Klebe⁴¹. For concentrations of substrate (Gsp1:GDP) that were much lower than the excess of mant-nucleotide (200 μ M) we used a combination of two exponential decays, and for reactions with high concentrations of Gsp1, where the relative excess of mant-nucleotide was lower, we always estimated the initial rates using linear fits to the very beginning of the

reaction, when levels of mant-nucleotide-bound Gsp1 are very low and therefore exchange is overwhelmingly from Gsp1-GDP to Gsp1-mant-nucleotide.

All kinetic measurements were done at 30°C in 100 µl reaction volume using 5 nM GEF ($\Delta 1\text{-}27Srm1$), except for higher concentrations of the mutants with high K_m values that were measured at 20 nM GEF. Data were collected in a Synergy H1 plate reader from BioTek, using Corning 3686 96-well half-area non-binding surface plates. For low concentrations of Gsp1:GDP the time course data were fit to a combination of two exponential decays:

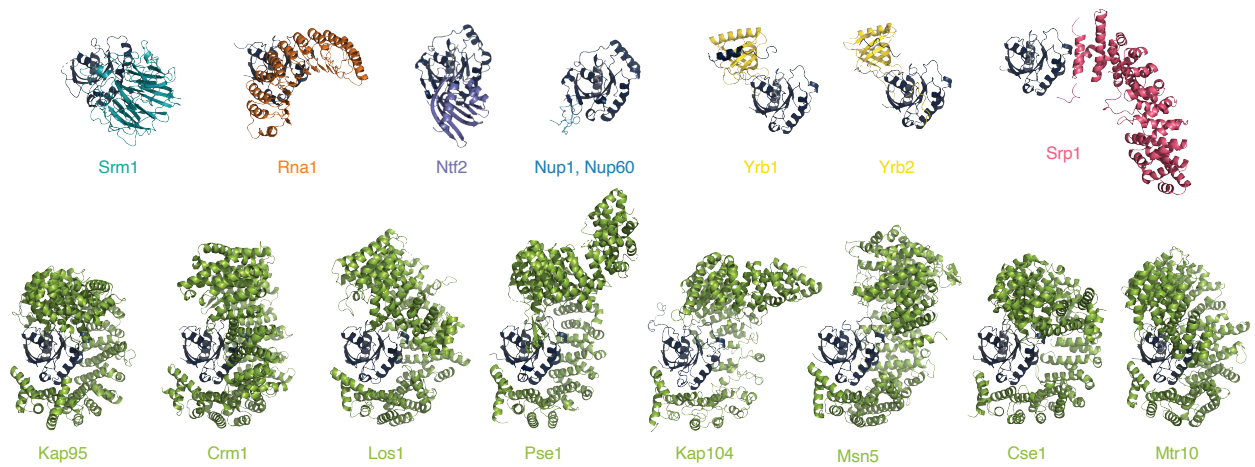
$$Y = \text{span1} * \exp(k_{\text{nucleotide exchange}} * \text{Time}) + \text{span2} * \exp(k_{\text{background}} * \text{Time}) + \text{fluorescence}_{\text{plateau}}$$

where $k_{\text{nucleotide exchange}}$ is the rate constant of the GDP to mant-GTP exchange, $k_{\text{background}}$ is the rate constant of background decay due to photo-bleaching, and span1 and span2 are the fluorescence amplitudes for the two processes. For high concentrations of substrate, or for mutants with very low rates, the initial velocity was determined by a linear fit to the initial 10–20% of the data. As the intrinsic exchange rate in the absence of GEF is estimated to be more than 10^4 lower⁴⁵ we do not use the intrinsic rate for fitting the data. The kinetic parameters of the nucleotide exchange were determined by fitting a Michaelis-Menten equation to an average of 38 data points (ranging from 17 to 91) per Gsp1 point mutant for a range of substrate concentrations from $[\text{Gsp1:GDP}] = 0.25 \mu\text{M}$ to $[\text{Gsp1:GDP}] \gg K_m$. Michaelis-Menten fits are shown in **Supplementary Fig. 4**. Michaelis-Menten k_{cat} and K_m parameters for GEF-mediated nucleotide exchange are provided in **Supplementary Table 7**. The errors of the k_{cat} and the K_m parameters were determined from the standard error of the exponential fit of the Michaelis-Menten equation to the data. The error of the catalytic efficiency (k_{cat}/K_m) was calculated by adding the standard errors of the individual parameters and normalizing it for the values of the

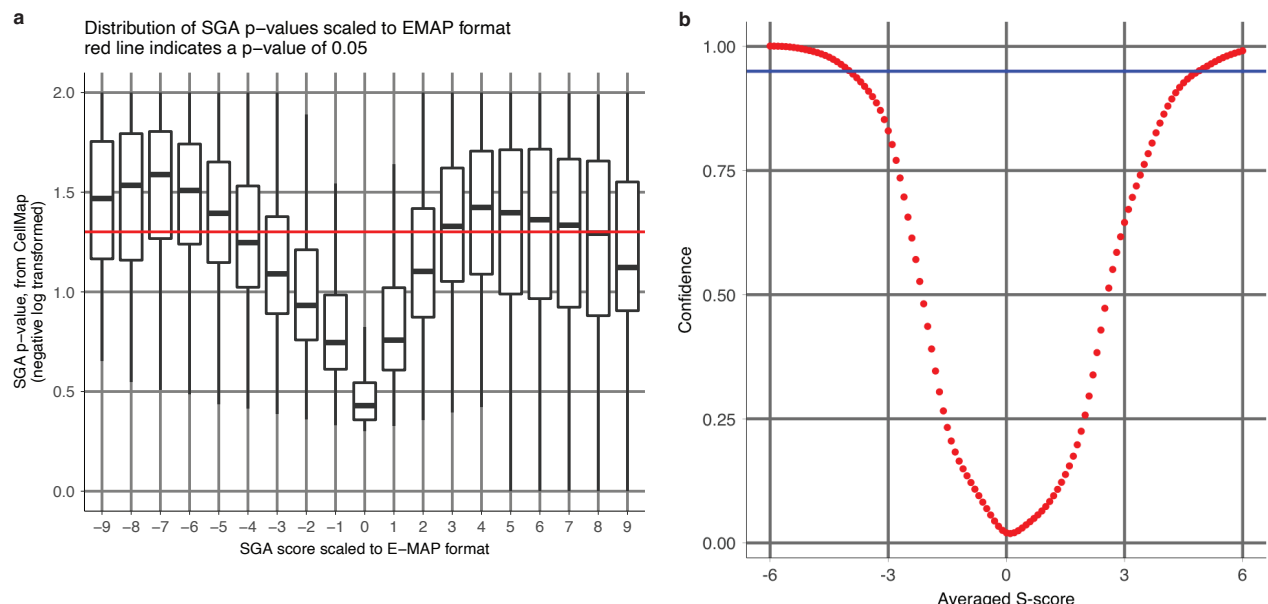
parameters ($k_{\text{cat}}/K_m \sqrt{\left(\frac{\text{std. error}(k_{\text{cat}})}{k_{\text{cat}}}\right)^2 + \left(\frac{\text{std. error}(K_m)}{K_m}\right)^2}$). All custom

code for fitting and analysis of kinetics data is provided in the accompanying repository (https://github.com/tinaperica/Gsp1_manuscript/tree/master/Scripts/kinetics). For more details on the kinetic analysis see **Supplementary Discussion**.

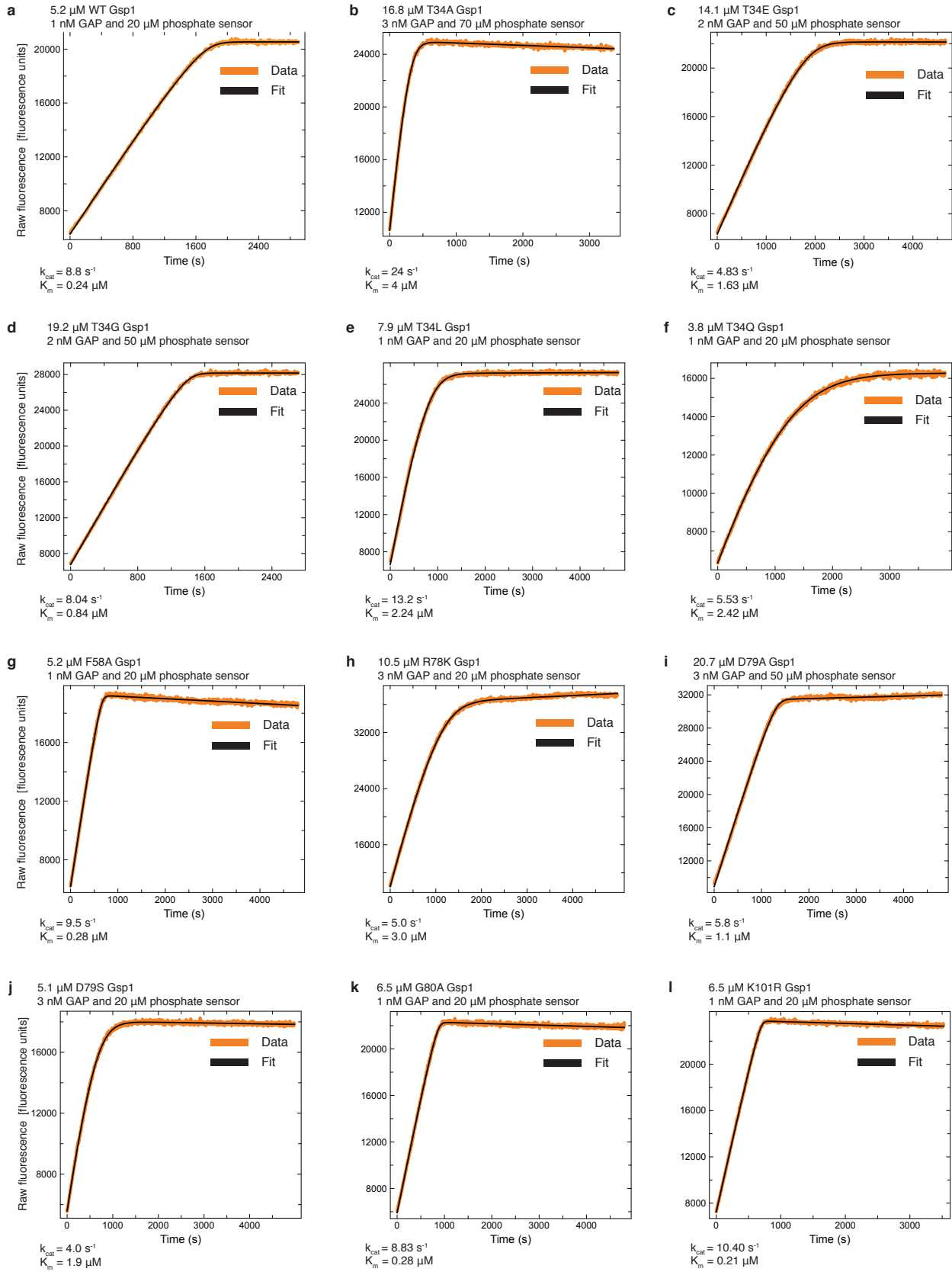
Supplementary Figures

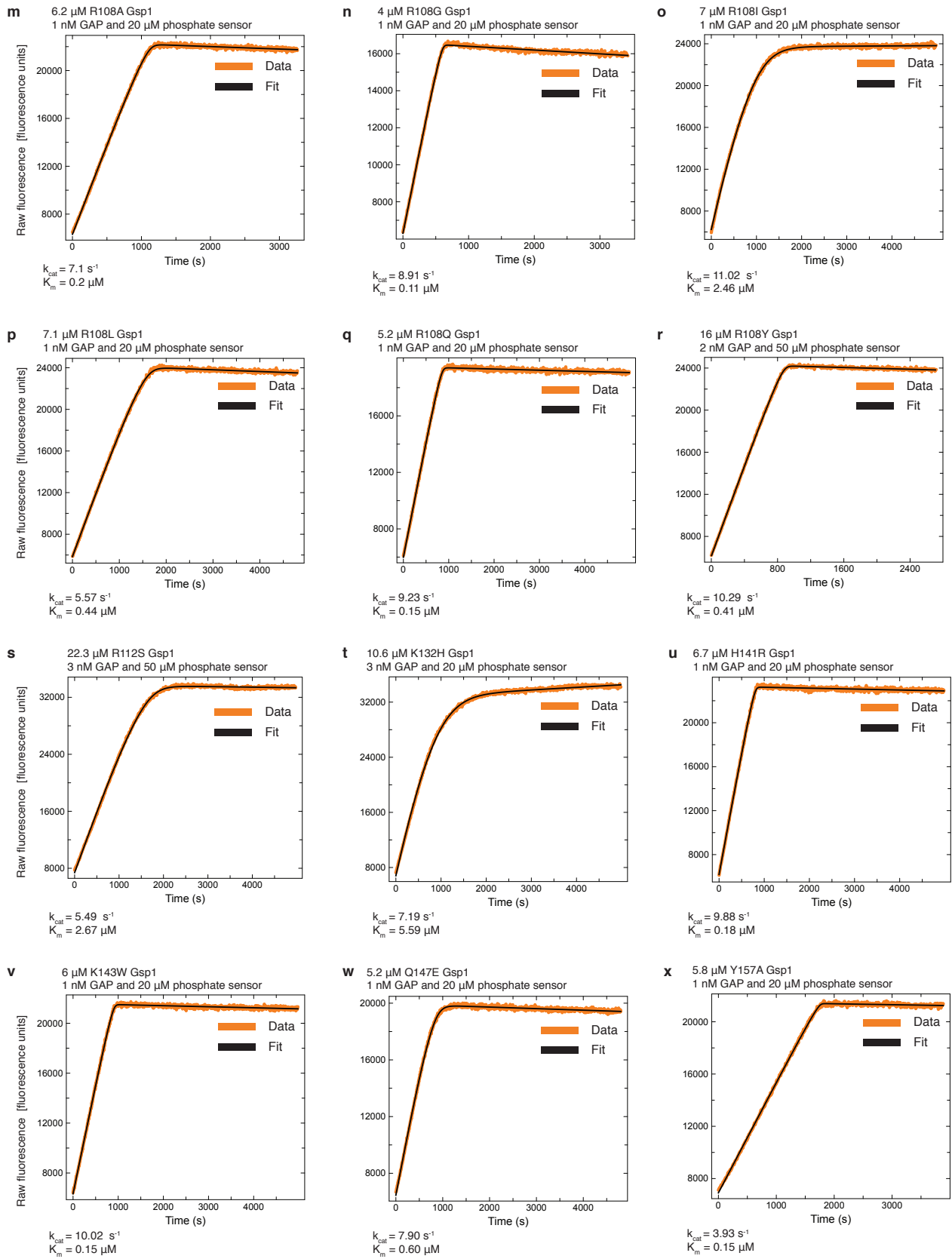


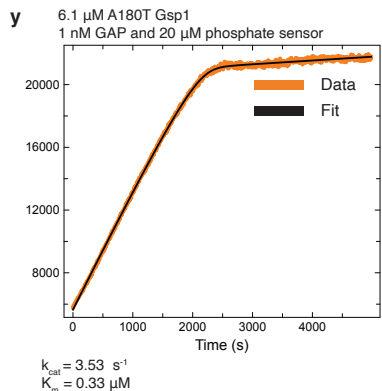
Supplementary Figure 1 Cartoon representation of co-complex structures of *S. cerevisiae* Gsp1 (dark navy) with indicated partners (or homologs). Srm1 (PDB 1I2M), Rna1 (PDB 1K5D), Ntf2 (PDB 1A2K), Nup1/Nup60 (PDB 3CH5), Yrb1 (PDB 3M1I), Yrb2 (PDB 3WYF), Srp1 (PDB 1WA5), Kap95 (PDB 2BKU), Crm1 (PDB 3M1I), Los1 (PDB 3ICQ), Pse1(PDB 3W3Z), Kap104 (PDB 1QBK), Msn5 (PDB 3A6P), Cse1 (PDB 1WA5), Mtr10 (PDB 4OL0). Species and sequence identity to *S. cerevisiae* homologs for these structures are provided in **Supplementary Table 1**.



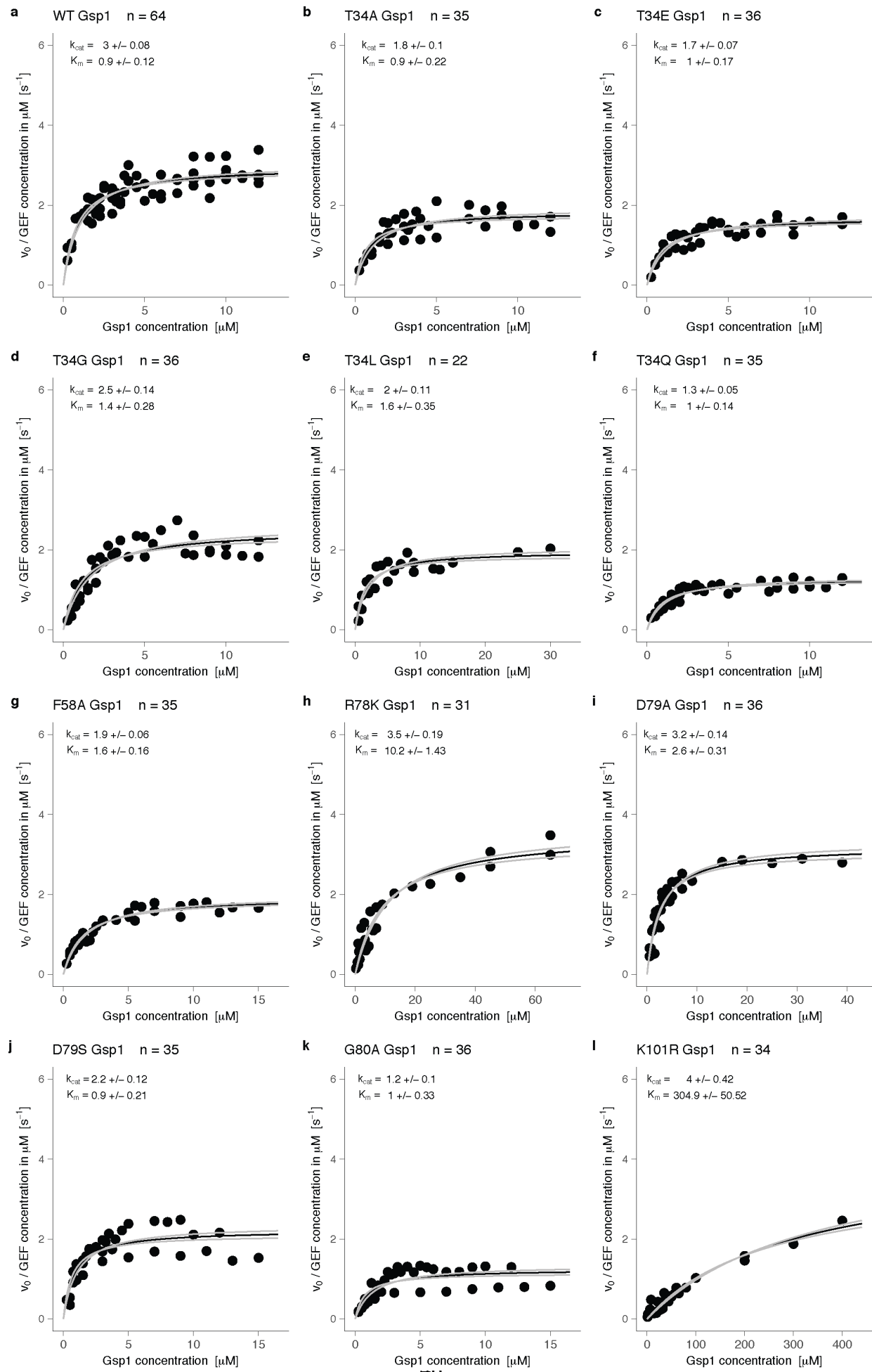
Supplementary Figure 2 Comparison of definitions of high confidence S-scores used in our analysis. **a**, Distribution of the SGA scores scaled to the E-MAP S-scores versus their corresponding published p-values from the CellMap¹⁴. **b**, Distribution of the E-MAP S-score averaged from all the individual replicates versus the confidence of the functional genetic interaction reproduced from Collins et al⁵.

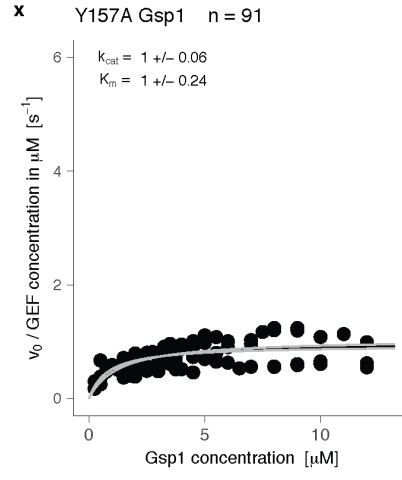
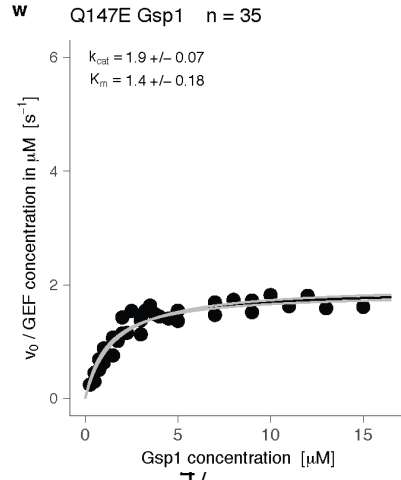
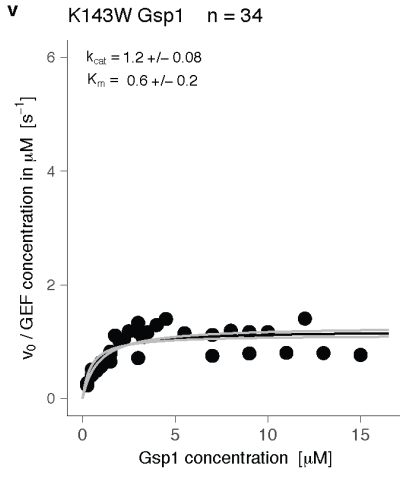
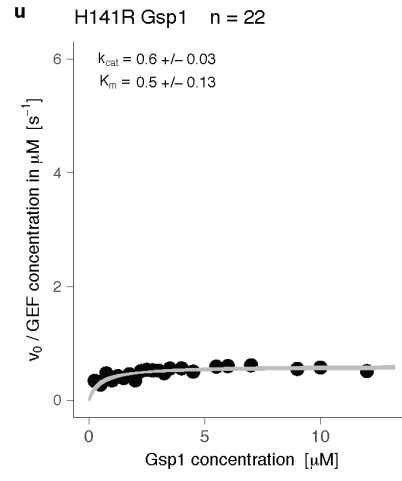
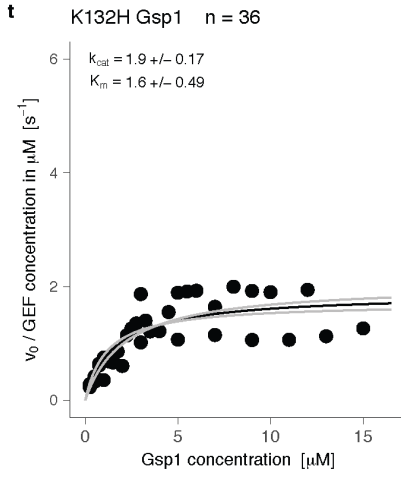
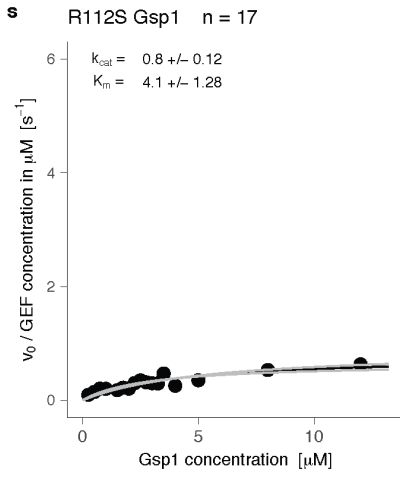
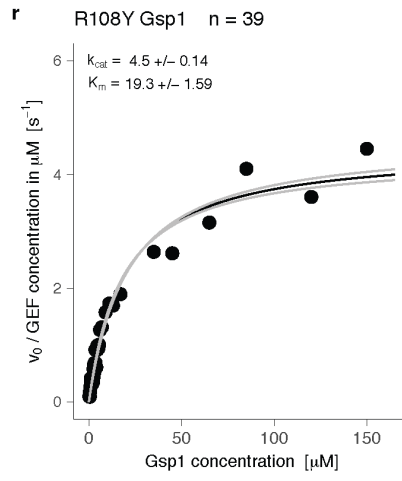
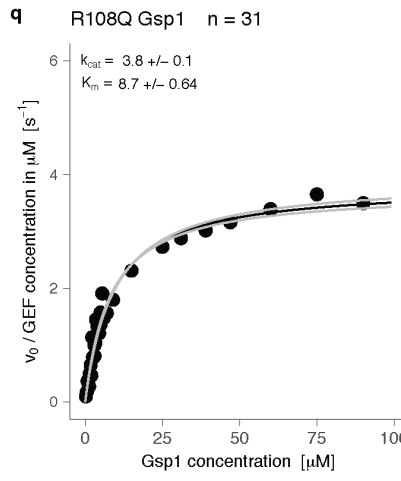
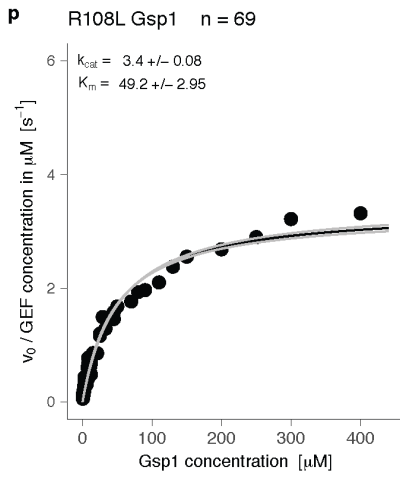
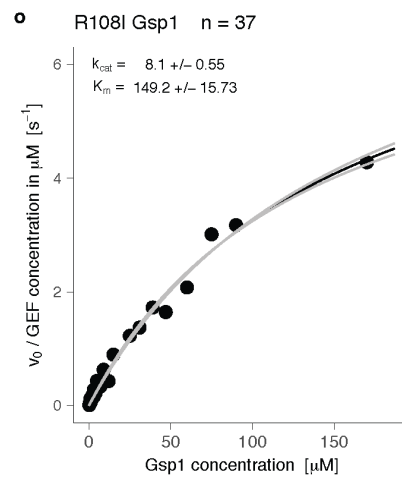
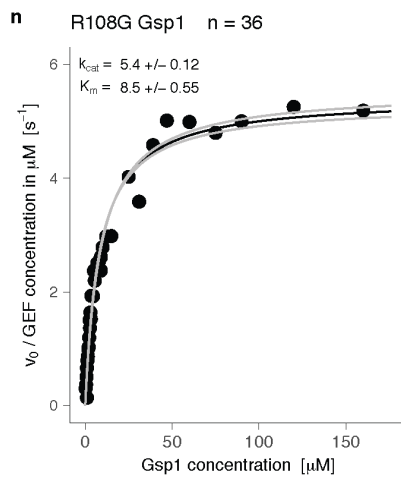
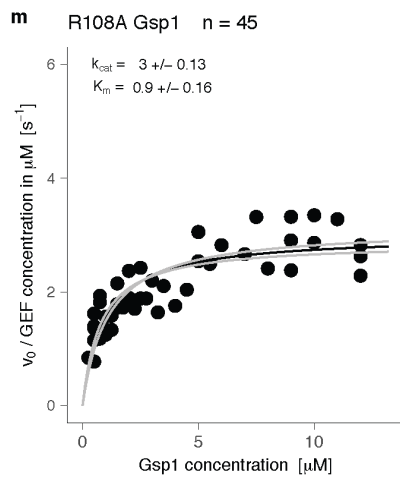


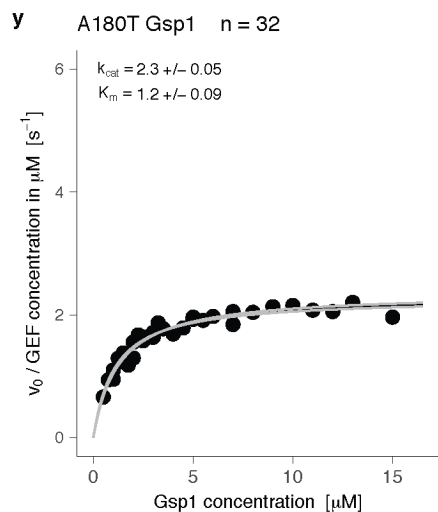




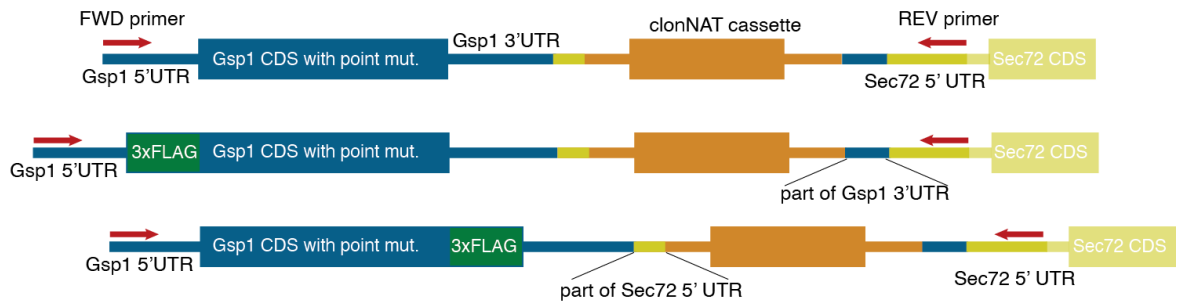
Supplementary Figure 3 GAP-mediated GTP hydrolysis monitored as fluorescence increase upon binding of released free phosphate to a fluorescent phosphate sensor. Curves were fit with the integrated Michaelis-Menten equation using the DELA software. Final Michaelis-Menten kinetic parameters (k_{cat} and K_m) for each Gsp1 mutant were calculated from three to nine individually fit curves as the ones shown in this figure. **a**, Wild type Gsp1, **b-y**, Gsp1 point mutants.



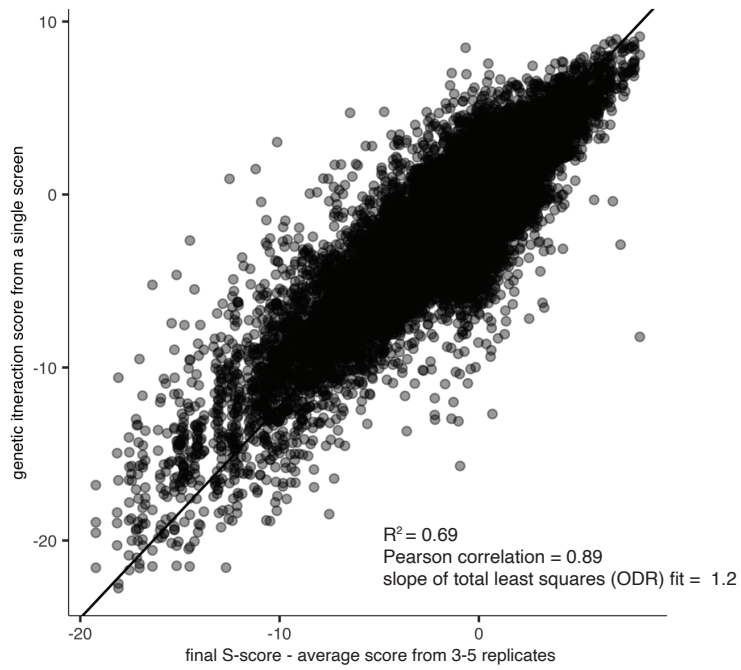




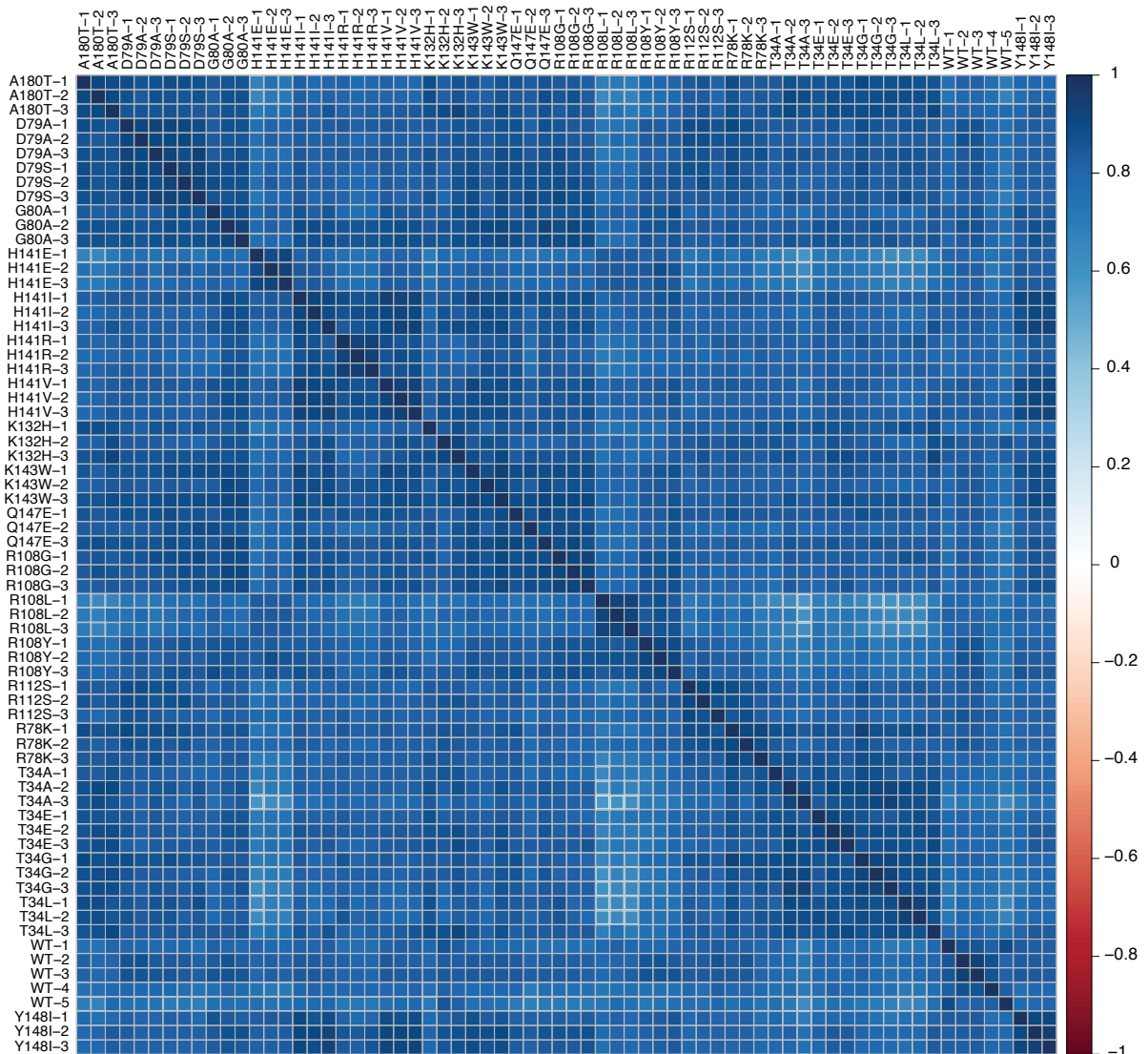
Supplementary Figure 4 Michaelis-Menten plots for GEF-mediated nucleotide exchange. Black line represents the Michaelis-Menten fit, and the gray lines represent the plus and minus one standard error of the fit. **a**, Wild type Gsp1. **b-y**, Gsp1 point mutants.



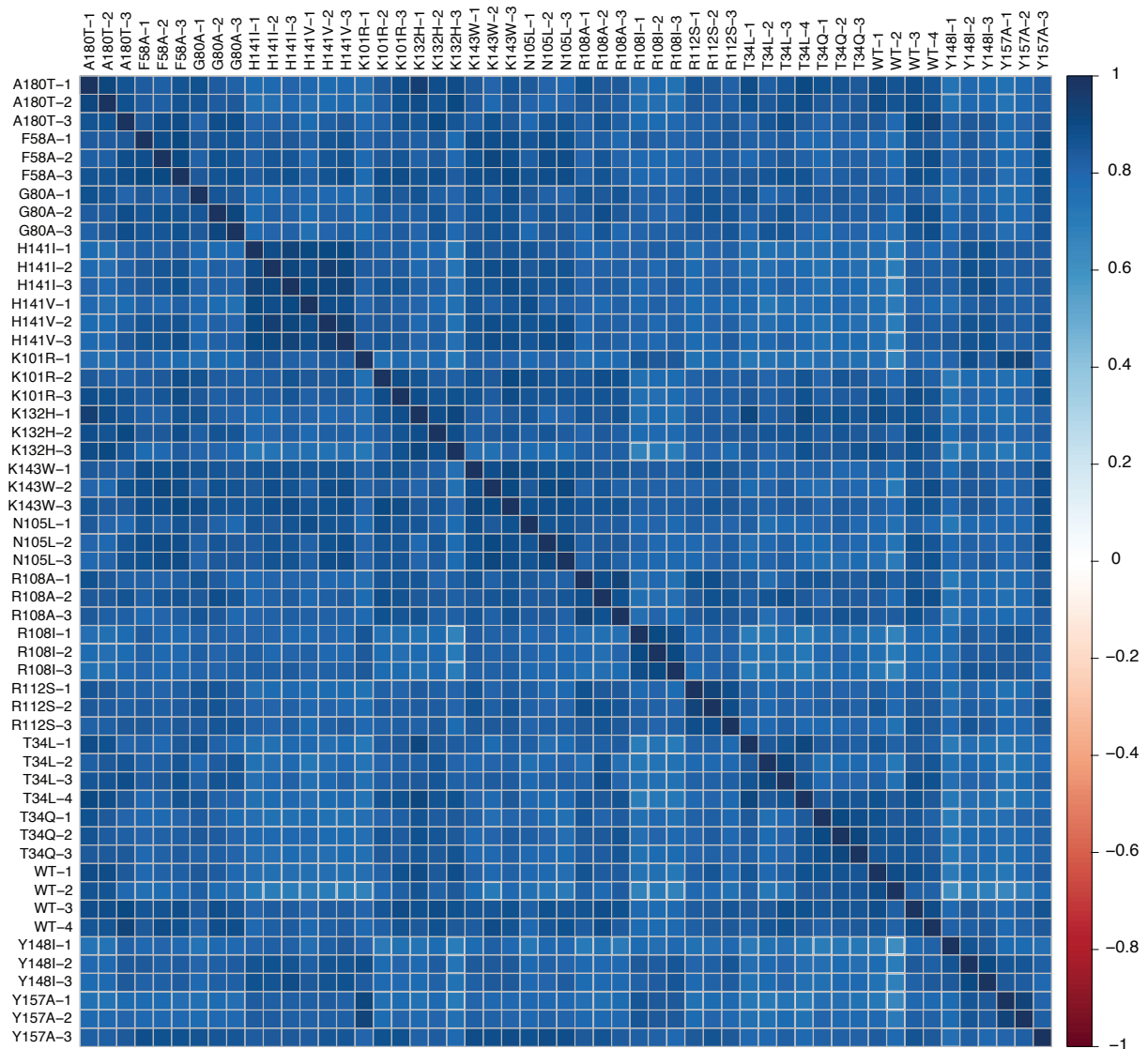
Supplementary Figure 5 Schematic of genetically integrated *GSP1* constructs. For E-MAP experiments, wild type or mutant *GSP1* cassettes including the clonNAT resistance cassette were integrated into the MAT: α strain. For AP-MS the constructs also included either an amino- (N) terminal or a carboxy- (C) terminal 3xFLAG tag (MDYKDHDG DYKDHDIDYKDDDKGGGGA and GGGGADYKDHDG DYKDHDIDYKDDDK, respectively).



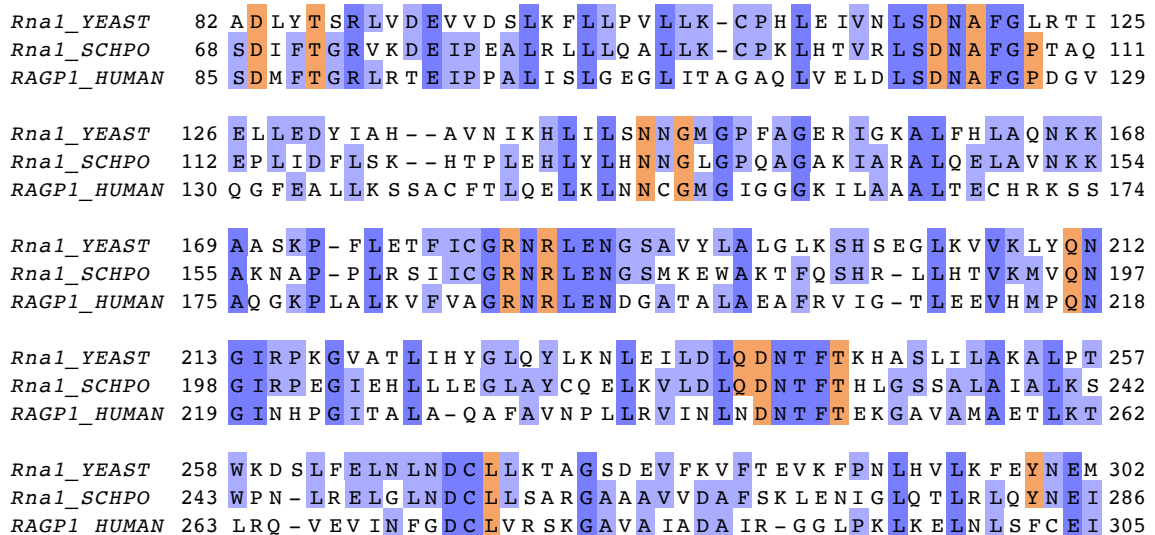
Supplementary Figure 6 Reproducibility of GSP1 point mutant E-MAP screens. A linear relationship between the genetic interaction S-score from a single E-MAP experiment and the final average S-score based on three or more replicates. The linear fit was calculated using the *odregress* function from the *pracma* R package.



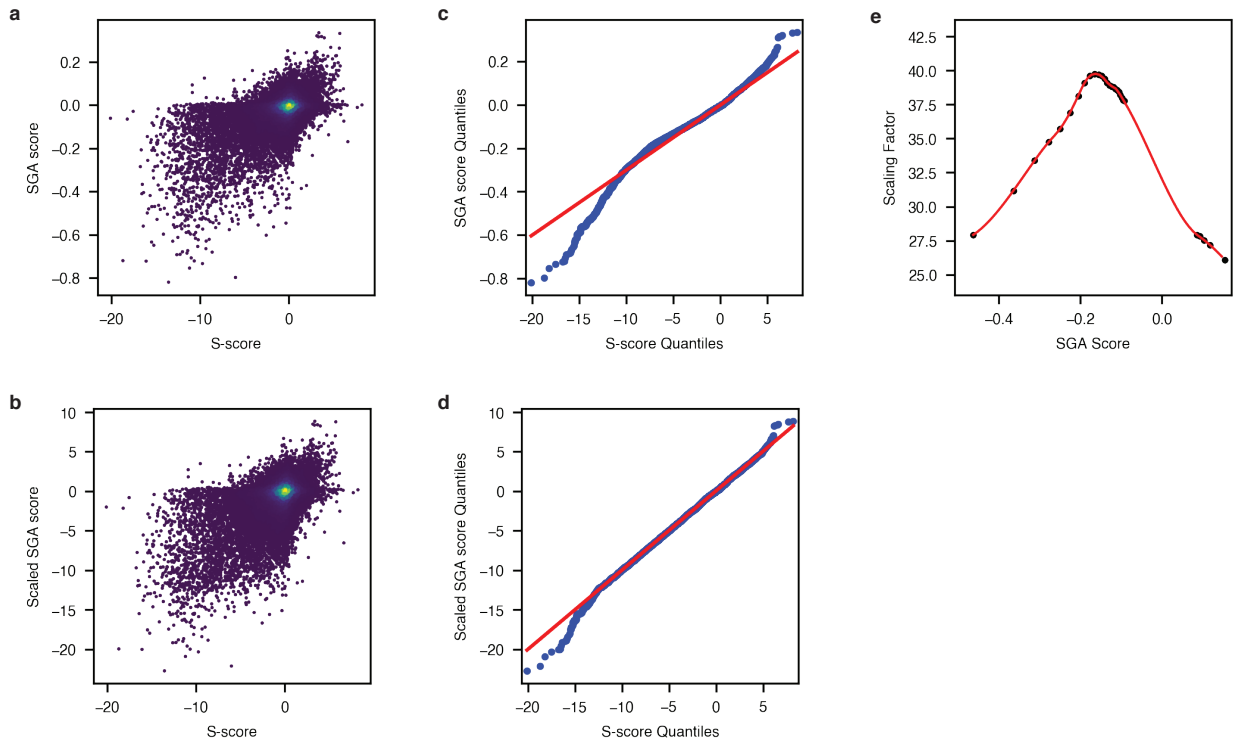
Supplementary Figure 7 Clustering of individual AP-MS replicates based on correlations between protein abundance before the final scoring. Data shown are for amino-terminally FLAG tagged wild type (WT) and Gsp1 mutants.



Supplementary Figure 8 Clustering of individual AP-MS replicates based on correlations between protein abundance before the final scoring. Data shown are for carboxy-terminally FLAG tagged wild type (WT) and Gsp1 mutants.

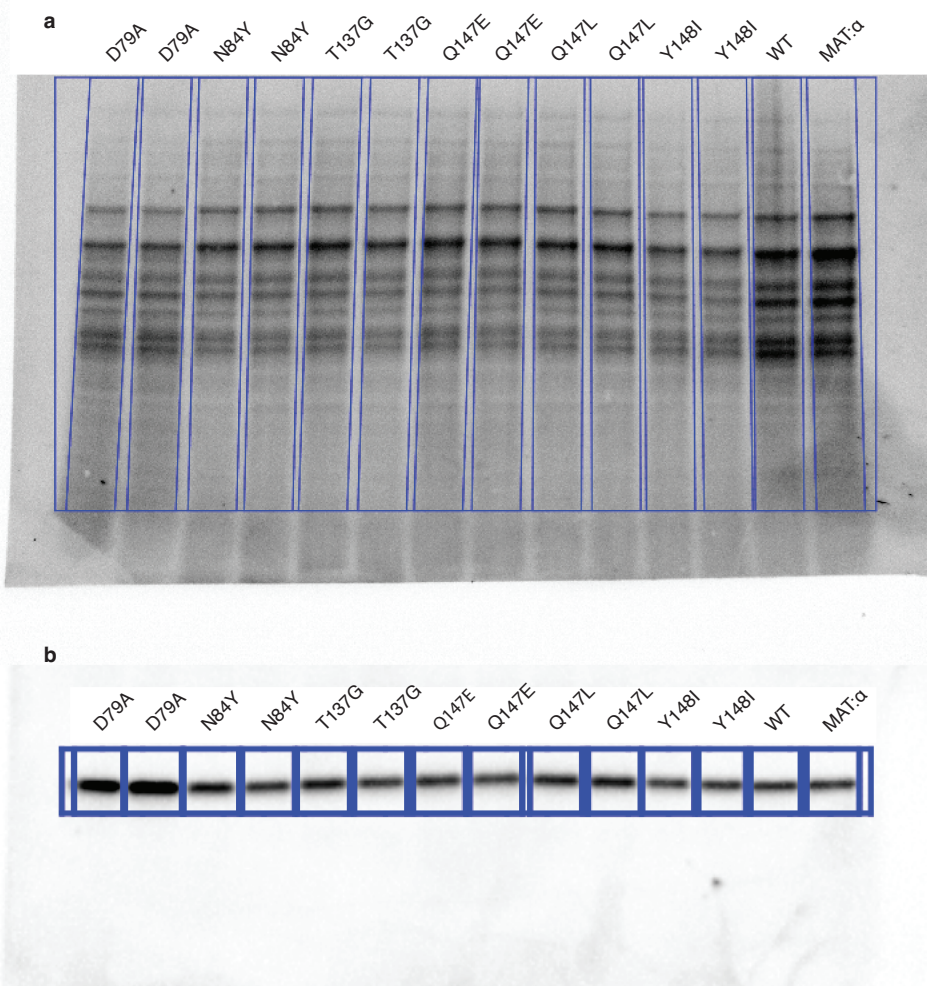


Supplementary Figure 9 Multiple sequence alignment between Rna1 from *S. cerevisiae* (*Rna1_YEAST*) and *S. pombe* (*Rna1_SCHPO*), as well as human RanGAP (*RAGP1_HUMAN*, excluding the C-terminal SUMO conjugation domain which is absent in Fungi). Overall sequence identity between *S. cerevisiae* and *S. pombe* Rna1 is 39%, with 53% sequence similarity. Interface core residues (based on the X-ray crystal structure between *S. pombe* Rna1 and mammalian Ran, PDB ID: 1k5d) are highlighted in orange. All interface core residues except Pro108 in *S. pombe* Rna1, which corresponds to Leu122 in *S. cerevisiae* Rna1, are conserved in sequence between *S. cerevisiae* and *S. pombe* Rna1.

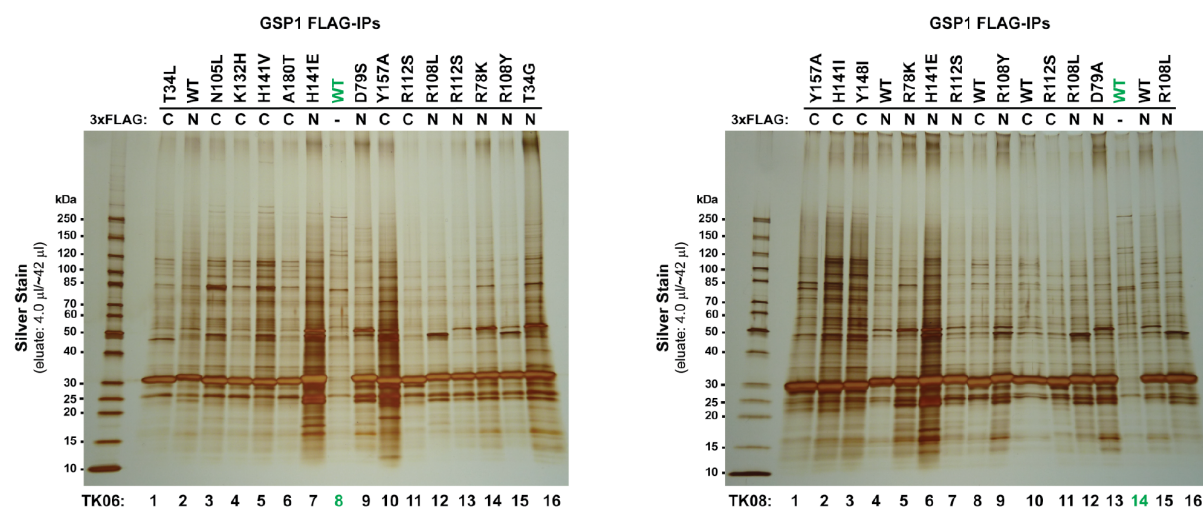


Supplementary Figure 10 Non-linear scaling of SGA data from the Cell Map to E-MAP format.

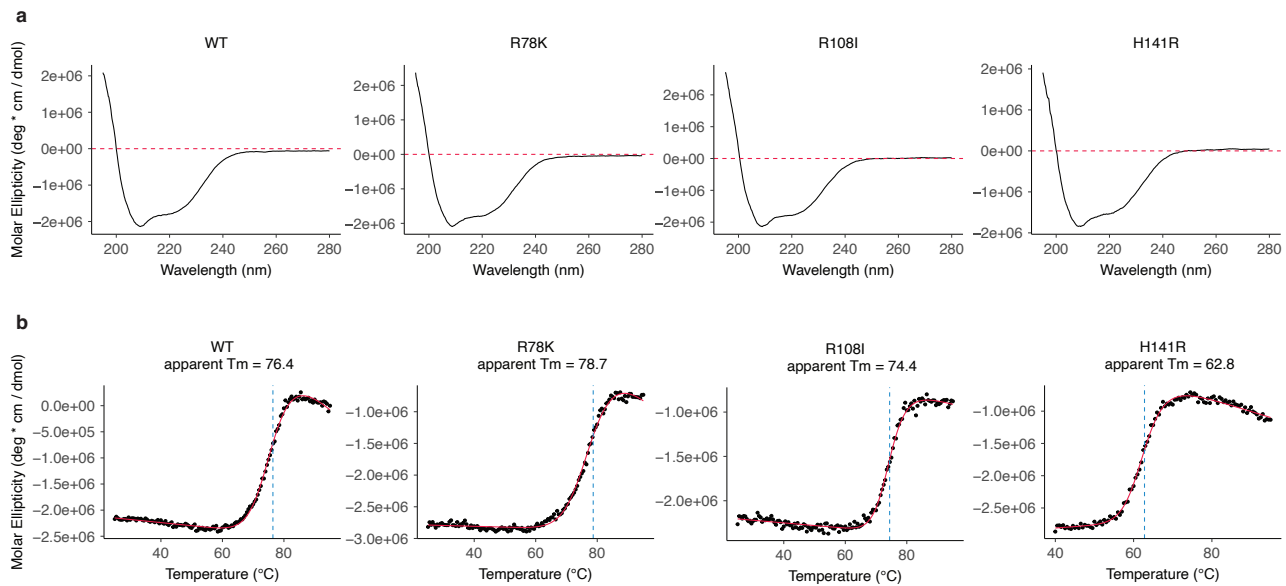
a, Distribution of S-scores from the chromatin biology E-MAP dataset²⁶ and the SGA score from the CellMap dataset¹⁴. **b**, Distribution of S-scores from the chromatin biology E-MAP dataset and the *scaled* SGA score from the CellMap dataset. **c**, Quantile-quantile plot showing the distribution of genetic interaction scores from the CellMap before scaling and the E-MAP chromatin biology datasets. **d**, Quantile-quantile plot showing the distribution of genetic interaction scores from the CellMap after scaling and the E-MAP chromatin biology dataset. **e**, The scaling function applied to the CellMap data. Red curve is the fitted spline of the scaling factors between the E-MAP S-scores and the SGA scores. Black dots represent the individual bins.



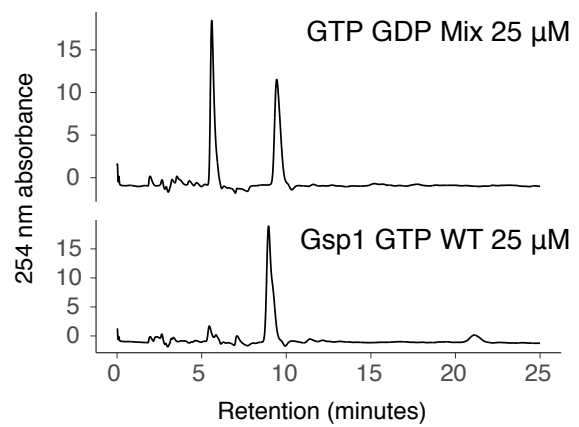
Supplementary Figure 11 Example data for Gsp1 protein expression estimation by Western blot.
a, Total protein staining. **b**, Western blot of starting *S. cerevisiae* strain (MAT: α , see **Supplementary Methods** for full strain description), wild type Gsp1 with clonNAT resistance marker (WT), and its mutants with anti-Ran antibody.



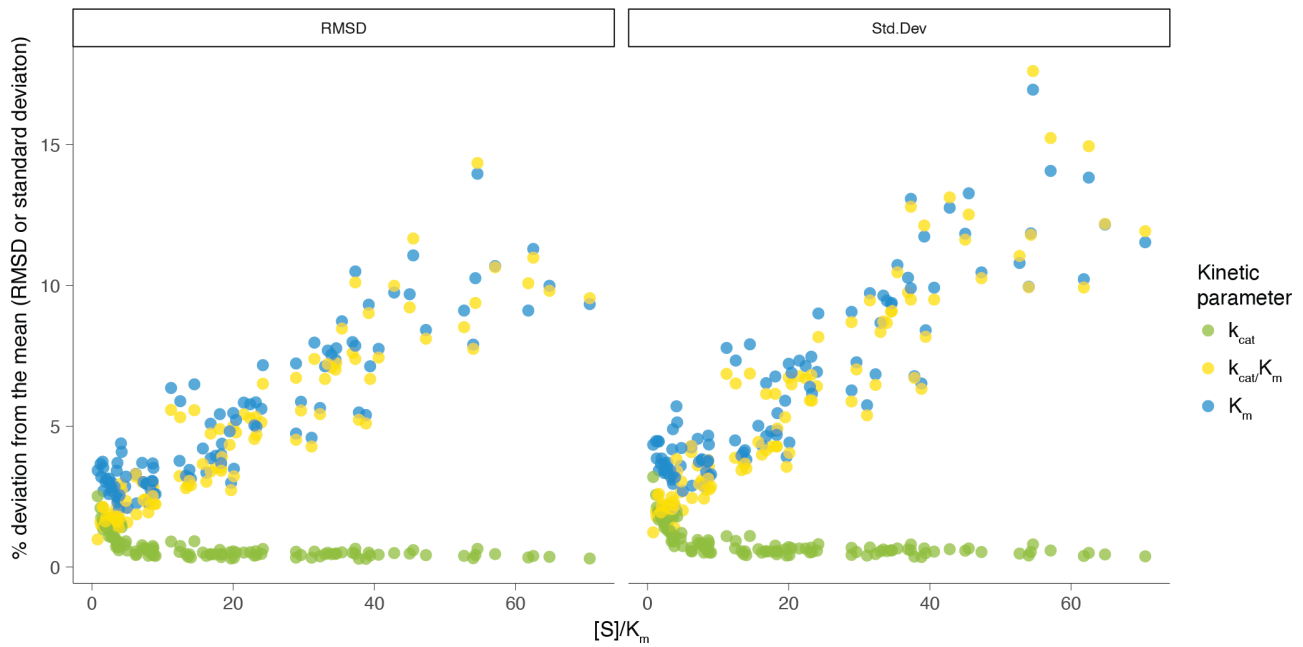
Supplementary Figure 12 Silver stain gels after FLAG immunoprecipitation of amino- (N) or carboxy- (C) terminally 3xFLAG tagged genetically integrated Gsp1. The strongest band at approximately 30 kDa corresponds to tagged Gsp1. Untagged wild type Gsp1 (lanes 8 and 14 in the left and right gel, respectively) were used as negative control for mass spectrometry analysis.



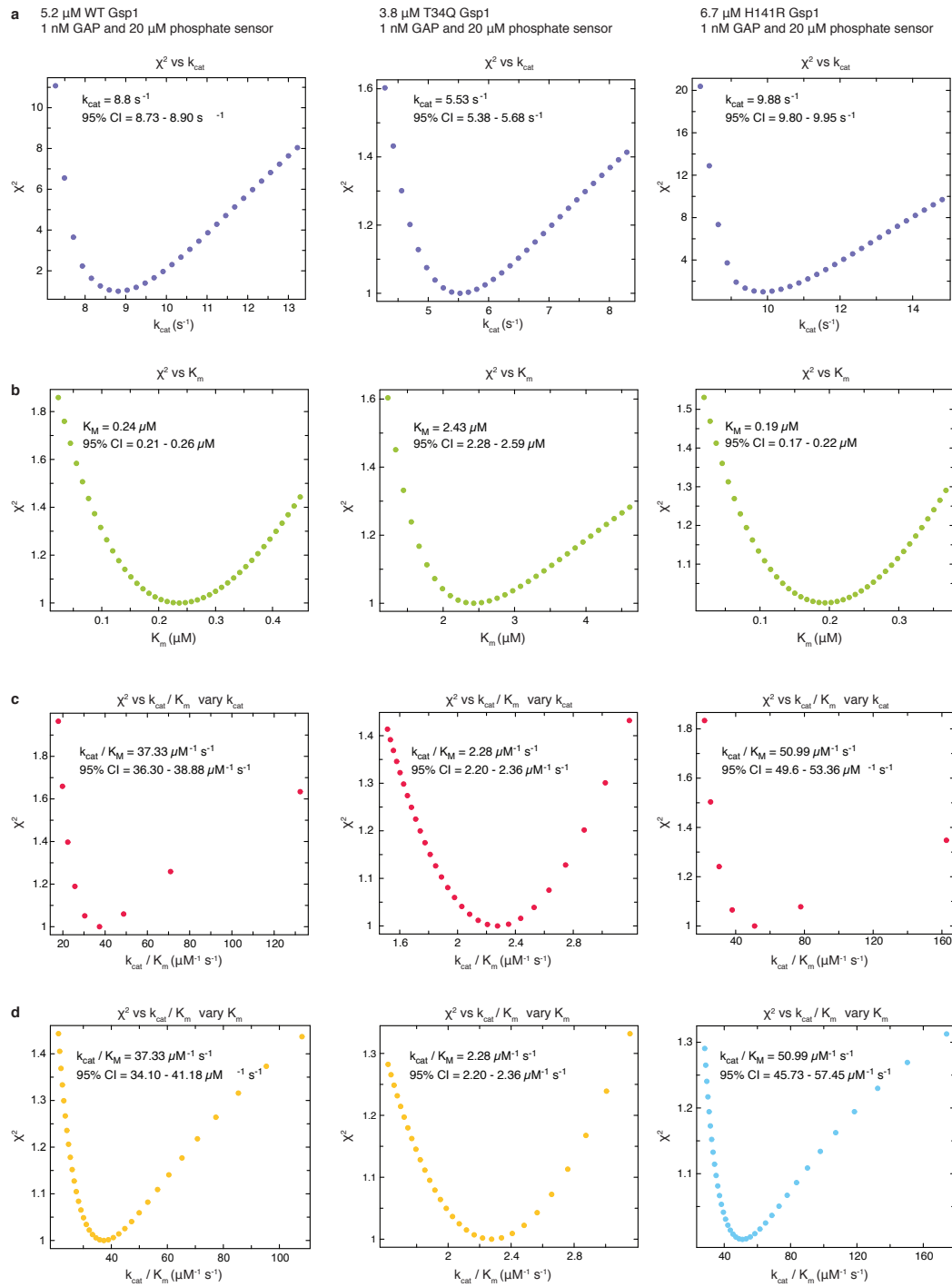
Supplementary Figure 13 Circular dichroism (CD) data for wild type (WT) Gsp1 and select mutants. a, CD spectra. b, Irreversible temperature melts.



Supplementary Figure 14 HPLC reverse phase chromatograms of a GTP/GDP mix (top) and that of a purified and GTP loaded wild type Gsp1 (bottom).



Supplementary Figure 15 Accuracy estimation for determining the kinetic parameters of GAP-mediated GTP hydrolysis from individual time courses spanning [S] > Km to [S] << Km fit with an accurate solution of the integrated Michaelis Menten (IMM) equation. Each time course was simulated using the experimentally determined parameters determined from the fitted IMM model, with added Gaussian noise similar to the experimental fluorescence signal noise. The deviation from the mean is plotted against a ratio of initial substrate (Gsp1:GTP) concentration [S] and the experimentally determined K_m. Deviation from the mean is reported either as standard deviation or RMSD = $\sqrt{\frac{\sum(\text{simulation_param} - \text{experimental_param})^2}{N}}$, where N = 100 simulations, and simulation_param and experimental_param are experimental and simulated k_{cat}, K_m, and k_{cat}/K_m, respectively. Here, simulated refers to the average of the fitted values for the simulated data sets.



Supplementary Figure 16 Estimated error around the maximum likelihood estimated values of the Michaelis-Menten parameters. Plotted is the change in χ^2 statistics as each of the parameters was fixed in gradual increments around the maximum likelihood value. The χ^2 values are relative to the maximum likelihood values. Error estimate analysis is shown for three of the Gsp1 variants: wild type Gsp1, the low efficiency Gsp1 T34Q mutant, and the high efficiency Gsp1 H141R mutant. 95% CI is the estimated 95% confidence interval for each value, based on the χ^2 surface. **a**, Change of χ^2 statistics as the k_{cat} value is varied around the maximum likelihood value. **b**, Change of χ^2 statistics as the K_m value is varied around the maximum likelihood value. **c**, Change of χ^2 statistics as the k_{cat}/K_m value is

varied around the maximum likelihood value and the K_m is kept fixed at the maximum likelihood value (k_{cat} is varied). **d**, Change of χ^2 statistics as the k_{cat}/K_m value is varied around the maximum likelihood value and the k_{cat} is kept fixed at the maximum likelihood value (K_m is varied).

Supplementary Tables

Supplementary Table 1 Co-complex X-ray crystal structures of Ran or Gsp1 with its partners.

| Ran/Gsp1 binding partner | | | | Ran/Gsp1 source species | Overall sequence identity to <i>S. cerevisiae</i> homolog | | Interface sequence identity to <i>S. cerevisiae</i> homolog | |
|--------------------------|--|------|----------------------|-------------------------|---|-------------|---|-------------|
| Gene name | Partner protein name / function | PDB | source species | | Gsp1 [%] | partner [%] | Gsp1 [%] | partner [%] |
| Srm1 | Guanine nucleotide exchange factor of Gsp1 (GEF) | 1I2M | <i>H. sapiens</i> | <i>H. sapiens</i> | 83 | 25 | 94 | 42 |
| Rna1 | Ran GTPase-activating protein 1 of Gsp1 (GAP) | 1K5D | <i>S. pombe</i> | <i>H. sapiens</i> | 83 | 39 | 84 | 71 |
| Ntf2 | Nuclear transport factor 2 | 1A2K | <i>R. norvegicus</i> | <i>C. lupus</i> | 83 | 40 | 89 | 44 |
| Nup1 | FG-repeat nucleoporin | 3CH5 | <i>R. norvegicus</i> | <i>H. sapiens</i> | 83 | 13 | 67 | 37 |
| Nup60 | FG-repeat nucleoporin | 3CH5 | <i>R. norvegicus</i> | <i>H. sapiens</i> | 83 | 8 | 67 | 37 |
| Yrb1 | Ran-specific GTPase-activating protein 1 | 3M1I | <i>S. cerevisiae</i> | <i>S. cerevisiae</i> | 100 | 100 | 100 | 100 |
| Yrb2 | Ran-specific GTPase-activating protein 2 | 3WYF | <i>S. cerevisiae</i> | <i>S. cerevisiae</i> | 100 | 100 | 100 | 100 |
| Srp1 | Importin subunit alpha - receptor for simple and bipartite NLS | 1WA5 | <i>S. cerevisiae</i> | <i>C. lupus</i> | 83 | 100 | 67 | 100 |
| Kap95 | Importin subunit beta-1 - receptor for cNLS | 2BKU | <i>S. cerevisiae</i> | <i>C. lupus</i> | 83 | 100 | 94 | 100 |
| Crm1 | Exportin-1 - Receptor for the leucine-rich nuclear export signal (NES) | 3M1I | <i>S. cerevisiae</i> | <i>S. cerevisiae</i> | 100 | 100 | 100 | 100 |
| Los1 | Exportin-T - tRNA nucleus export | 3ICQ | <i>S. pombe</i> | <i>S. cerevisiae</i> | 100 | 22 | 100 | 30 |
| Pse1 | Importin subunit beta-3 - receptor for cNLS and rg-NLS | 3W3Z | <i>S. cerevisiae</i> | <i>C. lupus</i> | 83 | 100 | 89 | 100 |
| Kap104 | Importin subunit beta-2 - receptor for rg-NLS and PY-NLS | 1QBK | <i>H. sapiens</i> | <i>H. sapiens</i> | 83 | 31 | 92 | 43 |
| Msn5 | Exportin and importin of proteins and tRNA | 3A6P | <i>H. sapiens</i> | <i>C. lupus</i> | 83 | 18 | 89 | 29 |
| Cse1 | Importin alpha re-exporter - export receptor for Srp1 | 1WA5 | <i>S. cerevisiae</i> | <i>C. lupus</i> | 83 | 100 | 89 | 100 |
| Mtr10 | mRNA transport regulator | 4OL0 | <i>H. sapiens</i> | <i>H. sapiens</i> | 83 | 21 | 88 | 36 |

Supplementary Table 2 Mutated residues in Gsp1 and their interface position and ΔrASA.

CellMap alleles are annotated in parentheses.

| Gsp1 residue number | Crm1 | Cse1 (cse1-5002) | Kap104 | Kap95 (kap95-e126k) | Los1 (los1) | Msn5 (msn5) |
|---------------------|----------------|------------------|----------------|---------------------|----------------|-------------|
| 34 | | | | rim / 0.1 | | |
| 58 | | | | | | |
| 78 | rim / 0.1 | core / 0.34 | core / 0.44 | core / 0.2 | rim / 0.33 | rim / 0.18 |
| 79 | core / 0.3 | core / 0.29 | support / 0.12 | core / 0.37 | support / 0.16 | core / 0.28 |
| 80 | core / 0.31 | core / 0.27 | core / 0.42 | core / 0.29 | core / 0.37 | core / 0.32 |
| 84 | rim / 0.3 | rim / 0.21 | rim / 0.3 | rim / 0.41 | rim / 0.09 | rim / 0.09 |
| 101 | rim / 0.17 | | | | rim / 0.13 | rim / 0.02 |
| 102 | support / 0.01 | | | | core / 0.08 | |
| 105 | rim / 0.06 | | | rim / 0.03 | rim / 0.16 | core / 0.25 |
| 108 | core / 0.26 | rim / 0.1 | rim / 0.11 | rim / 0.12 | core / 0.43 | core / 0.42 |
| 112 | core / 0.55 | core / 0.45 | core / 0.44 | core / 0.56 | core / 0.4 | core / 0.58 |
| 115 | rim / 0.25 | rim / 0.2 | rim / 0.27 | rim / 0.07 | rim / 0.34 | rim / 0.34 |
| 129 | | rim / 0.61 | rim / 0.59 | rim / 0.19 | | rim / 0.23 |
| 132 | core / 0.12 | rim / 0 | | | rim / 0.03 | rim / 0.12 |
| 137 | | | | | | |
| 139 | rim / 0.01 | | | core / 0.04 | rim / 0.02 | |
| 141 | support / 0.14 | | support / 0.19 | core / 0.15 | | |
| 143 | rim / 0.48 | rim / 0.15 | core / 0.35 | rim / 0.27 | rim / 0.09 | rim / 0.01 |
| 147 | core / 0.23 | | support / 0.23 | core / 0.25 | core / 0.07 | core / 0.14 |
| 148 | support / 0.11 | support / 0.03 | support / 0.13 | | support / 0.01 | |
| 154 | | core / 0.28 | | core / 0.38 | rim / 0.13 | |
| 157 | core / 0.38 | rim / 0.13 | core / 0.39 | core / 0.29 | rim / 0.05 | |
| 169 | rim / 0.21 | | | rim / 0.02 | | rim / 0.17 |
| 180 | | | rim / 0.01 | | | |

Supplementary Table 2 (continued) Mutated residues in Gsp1 and their interface position

and ΔrASA. CellMap alleles are annotated in parentheses.

| Gsp1 residue number | Mtr10 | Ntf2 (ntf2-h104y, ntf2-5001) | Nup1 | Nup60 | Pse1 | Rna1 (rna1-1, rna1-s116f) |
|---------------------|----------------|------------------------------|----------------|----------------|----------------|---------------------------|
| 34 | | | | | | |
| 58 | | | rim / 0.28 | rim / 0.28 | | |
| 78 | core / 0.25 | core / 0.57 | rim / 0 | rim / 0 | support / 0.03 | support / 0.02 |
| 79 | core / 0.36 | rim / 0.1 | | | core / 0.26 | |
| 80 | core / 0.51 | core / 0.27 | support / 0.13 | support / 0.13 | core / 0.51 | |
| 84 | rim / 0.36 | | rim / 0.25 | rim / 0.25 | rim / 0.2 | |
| 101 | | | | | | rim / 0.01 |
| 102 | support / 0.1 | | | | | support / 0.07 |
| 105 | core / 0.21 | | | | | |
| 108 | core / 0.18 | | | | rim / 0.12 | |
| 112 | core / 0.57 | | | | core / 0.46 | |
| 115 | rim / 0.12 | | | | rim / 0.37 | |
| 129 | | | | | | rim / 0 |
| 132 | | | | | | core / 0.44 |
| 137 | core / 0.08 | | | | | rim / 0.01 |
| 139 | rim / 0.15 | | | | core / 0.18 | |
| 141 | core / 0.14 | | | | support / 0 | |
| 143 | core / 0.44 | | | | core / 0.52 | |
| 147 | support / 0.09 | | | | core / 0.09 | |
| 148 | support / 0.01 | | | | | |
| 154 | rim / 0.03 | | | | rim / 0.05 | |
| 157 | rim / 0.04 | | | | | |
| 169 | | | | | | |
| 180 | | | | | | |

Supplementary Table 2 (continued) Mutated residues in Gsp1 and their interface position**and ΔrASA.** CellMap alleles are annotated in parentheses.

| Gsp1 residue number | Srm1 (srm1-g282s, srm1-ts) | Srp1 (srp1-5001) | Yrb1 (yrb1-51) | Yrb2 |
|---------------------|----------------------------|------------------|----------------|-------------|
| 34 | | | core / 0.4 | rim / 0.24 |
| 58 | | | core / 0.4 | core / 0.39 |
| 78 | rim / 0.46 | | | |
| 79 | rim / 0.01 | | | |
| 80 | | | | |
| 84 | | | | |
| 101 | core / 0.67 | core / 0.47 | | |
| 102 | support / 0.15 | | | |
| 105 | core / 0.44 | rim / 0.03 | | |
| 108 | core / 0.47 | | | |
| 112 | rim / 0.24 | | | |
| 115 | | | | |
| 129 | | rim / 0.1 | | |
| 132 | rim / 0.16 | core / 0.22 | | |
| 137 | | core / 0.2 | | |
| 139 | core / 0.26 | rim / 0.01 | | |
| 141 | | | | |
| 143 | rim / 0.07 | | | |
| 147 | | | | |
| 148 | | | | |
| 154 | | | | |
| 157 | | | | |
| 169 | | | | |
| 180 | | | core / 0.64 | rim / 0.5 |

Supplementary Table 3 Gsp1 mutants and attempted yeast constructs.

| construct name | Gsp1 residue number | Gsp1 point mutation | yeast strain successfully made |
|------------------------------|---------------------|---------------------|--------------------------------|
| C-terminal 3xFLAG GSP1 T34L | 34 | T34L | yes |
| C-terminal 3xFLAG GSP1 T34Q | 34 | T34Q | yes |
| GSP1 T34A | 34 | T34A | yes |
| GSP1 T34D | 34 | T34D | yes |
| GSP1 T34E | 34 | T34E | yes |
| GSP1 T34G | 34 | T34G | yes |
| GSP1 T34L | 34 | T34L | yes |
| GSP1 T34Q | 34 | T34Q | yes |
| GSP1 T34S | 34 | T34S | yes |
| GSP1 T34Y | 34 | T34Y | yes |
| N-terminal 3xFLAG GSP1 T34A | 34 | T34A | yes |
| N-terminal 3xFLAG GSP1 T34E | 34 | T34E | yes |
| N-terminal 3xFLAG GSP1 T34G | 34 | T34G | yes |
| N-terminal 3xFLAG GSP1 T34L | 34 | T34L | yes |
| C-terminal 3xFLAG GSP1 F58A | 58 | F58A | yes |
| GSP1 F58A | 58 | F58A | yes |
| GSP1 F58L | 58 | F58L | yes |
| GSP1 R78K | 78 | R78K | yes |
| N-terminal 3xFLAG GSP1 R78K | 78 | R78K | yes |
| C-terminal 3xFLAG GSP1 D79A | 79 | D79A | yes |
| GSP1 D79A | 79 | D79A | yes |
| GSP1 D79S | 79 | D79S | yes |
| N-terminal 3xFLAG GSP1 D79A | 79 | D79A | yes |
| N-terminal 3xFLAG GSP1 D79S | 79 | D79S | yes |
| C-terminal 3xFLAG GSP1 G80A | 80 | G80A | yes |
| GSP1 G80A | 80 | G80A | yes |
| N-terminal 3xFLAG GSP1 G80A | 80 | G80A | yes |
| GSP1 N84Y | 84 | N84Y | yes |
| C-terminal 3xFLAG GSP1 K101R | 101 | K101R | yes |
| GSP1 K101R | 101 | K101R | yes |
| GSP1 N102I | 102 | N102I | yes |
| GSP1 N102K | 102 | N102K | yes |
| GSP1 N102M | 102 | N102M | yes |
| C-terminal 3xFLAG GSP1 N105L | 105 | N105L | yes |
| GSP1 N105L | 105 | N105L | yes |
| GSP1 N105V | 105 | N105V | yes |
| C-terminal 3xFLAG GSP1 R108A | 108 | R108A | yes |
| C-terminal 3xFLAG GSP1 R108I | 108 | R108I | yes |
| C-terminal 3xFLAG GSP1 R108Y | 108 | R108Y | yes |
| GSP1 R108A | 108 | R108A | yes |
| GSP1 R108D | 108 | R108D | yes |
| GSP1 R108G | 108 | R108G | yes |
| GSP1 R108I | 108 | R108I | yes |

Supplementary Table 3 (continued) Gsp1 mutants and attempted yeast constructs.

| construct name | Gsp1 residue number | Gsp1 point mutation | yeast strain successfully made |
|------------------------------|---------------------|---------------------|--------------------------------|
| GSP1 R108L | 108 | R108L | yes |
| GSP1 R108Q | 108 | R108Q | yes |
| GSP1 R108S | 108 | R108S | yes |
| GSP1 R108Y | 108 | R108Y | yes |
| N-terminal 3xFLAG GSP1 R108G | 108 | R108G | yes |
| N-terminal 3xFLAG GSP1 R108Y | 108 | R108Y | yes |
| C-terminal 3xFLAG GSP1 R112S | 112 | R112S | yes |
| GSP1 R112A | 112 | R112A | yes |
| GSP1 R112S | 112 | R112S | yes |
| N-terminal 3xFLAG GSP1 R112S | 112 | R112S | yes |
| GSP1 E115A | 115 | E115A | yes |
| GSP1 E115I | 115 | E115I | yes |
| GSP1 K129E | 129 | K129E | yes |
| GSP1 K129F | 129 | K129F | yes |
| GSP1 K129I | 129 | K129I | yes |
| GSP1 K129T | 129 | K129T | yes |
| C-terminal 3xFLAG GSP1 K132H | 132 | K132H | yes |
| GSP1 K132H | 132 | K132H | yes |
| N-terminal 3xFLAG GSP1 K132H | 132 | K132H | yes |
| GSP1 T137G | 137 | T137G | yes |
| GSP1 T139A | 139 | T139A | yes |
| GSP1 T139R | 139 | T139R | yes |
| C-terminal 3xFLAG GSP1 H141I | 141 | H141I | yes |
| C-terminal 3xFLAG GSP1 H141V | 141 | H141V | yes |
| GSP1 H141E | 141 | H141E | yes |
| GSP1 H141I | 141 | H141I | yes |
| GSP1 H141R | 141 | H141R | yes |
| GSP1 H141V | 141 | H141V | yes |
| N-terminal 3xFLAG GSP1 H141E | 141 | H141E | yes |
| N-terminal 3xFLAG GSP1 H141I | 141 | H141I | yes |
| N-terminal 3xFLAG GSP1 H141R | 141 | H141R | yes |
| N-terminal 3xFLAG GSP1 H141V | 141 | H141V | yes |
| C-terminal 3xFLAG GSP1 K143W | 143 | K143W | yes |
| GSP1 K143H | 143 | K143H | yes |
| GSP1 K143W | 143 | K143W | yes |
| GSP1 K143Y | 143 | K143Y | yes |
| N-terminal 3xFLAG GSP1 K143W | 143 | K143W | yes |
| GSP1 Q147E | 147 | Q147E | yes |
| GSP1 Q147L | 147 | Q147L | yes |
| N-terminal 3xFLAG GSP1 Q147E | 147 | Q147E | yes |
| C-terminal 3xFLAG GSP1 Y148I | 148 | Y148I | yes |

Supplementary Table 3 (continued) Gsp1 mutants and attempted yeast constructs.

| construct name | Gsp1 residue number | Gsp1 point mutation | yeast strain successfully made |
|------------------------------|---------------------|---------------------|--------------------------------|
| GSP1 Y148I | 148 | Y148I | yes |
| N-terminal 3xFLAG GSP1 Y148I | 148 | Y148I | yes |
| GSP1 K154M | 154 | K154M | yes |
| C-terminal 3xFLAG GSP1 Y157A | 157 | Y157A | yes |
| GSP1 Y157A | 157 | Y157A | yes |
| GSP1 K169I | 169 | K169I | yes |
| C-terminal 3xFLAG GSP1 A180T | 180 | A180T | yes |
| GSP1 A180T | 180 | A180T | yes |
| N-terminal 3xFLAG GSP1 A180T | 180 | A180T | yes |
| T34A Cter3xFL | 34 | T34A | no |
| T34E Cter3xFL | 34 | T34E | no |
| T34G Cter3xFL | 34 | T34G | no |
| T34Q Nter3xFL | 34 | T34Q | no |
| K39M | 39 | K39M | no |
| Y41A | 41 | Y41A | no |
| V49D | 49 | V49D | no |
| F58A Nter3xFL | 58 | F58A | no |
| G70N | 70 | G70N | no |
| Q71E | 71 | Q71E | no |
| K73Q | 73 | K73Q | no |
| G75N | 75 | G75N | no |
| R78K Cter3xFL | 78 | R78K | no |
| D79K | 79 | D79K | no |
| D79S Cter3xFL | 79 | D79S | no |
| G80N | 80 | G80N | no |
| G80S | 80 | G80S | no |
| I98F | 98 | I98F | no |
| K101R Nter3xFL | 101 | K101R | no |
| R108G Cter3xFL | 108 | R108G | no |
| R108I Nter3xFL | 108 | R108I | no |
| R108L Nter3xFL | 108 | R108L | no |
| R108Q Cter3xFL | 108 | R108Q | no |
| R108S Cter3xFL | 108 | R108S | no |
| K132M | 132 | K132M | no |
| K132Y | 132 | K132Y | no |
| T137E | 137 | T137E | no |
| H141E Cter3xFL | 141 | H141E | no |
| H141R Cter3xFL | 141 | H141R | no |
| Q147E Cter3xFL | 147 | Q147E | no |
| Y157K | 157 | Y157K | no |

Supplementary Table 4 Pearson correlations between Gsp1 mutants and the alleles of their direct interaction partners from the SGA CellMap. Ordered by correlation value.

| GSP1 mutant | Partner strain name | Pearson correlation coefficient | Residue in interface core | GSP1 mutant | Partner strain name | Pearson correlation coefficient | Residue in interface core |
|-------------|---------------------|---------------------------------|---------------------------|-------------|---------------------|---------------------------------|---------------------------|
| D79S | kap95-e126k | 0.4146 | TRUE | R108I | ntf2-5001 | 0.2544 | FALSE |
| Y148I | crm1_damp | 0.4027 | FALSE | D79A | srm1-ts | 0.251 | FALSE |
| R108L | ntf2-h104y | 0.3827 | FALSE | D79S | yrb1-51 | 0.2502 | FALSE |
| R108G | crm1_damp | 0.3783 | TRUE | H141I | ntf2-5001 | 0.2501 | FALSE |
| R108L | ntf2-5001 | 0.3612 | FALSE | T34G | cse1-5002 | 0.2467 | FALSE |
| R108Y | ntf2-h104y | 0.3612 | FALSE | D79A | ntf2-h104y | 0.2459 | FALSE |
| G80A | kap95-e126k | 0.3545 | TRUE | K101R | kap95-e126k | 0.2449 | FALSE |
| R112A | ntf2-h104y | 0.3533 | FALSE | T34Q | yrb1-51 | 0.241 | TRUE |
| R108Y | crm1_damp | 0.3453 | TRUE | G80A | ntf2-h104y | 0.2402 | TRUE |
| K101R | ntf2-h104y | 0.3389 | FALSE | T34G | kap95-e126k | 0.2365 | FALSE |
| R112S | ntf2-h104y | 0.3353 | FALSE | K101R | srm1-g282s | 0.2359 | TRUE |
| R108Q | crm1_damp | 0.3291 | TRUE | G80A | cse1-5002 | 0.2357 | TRUE |
| T34A | ntf2-5001 | 0.3231 | FALSE | Y148I | ntf2-h104y | 0.2355 | FALSE |
| Q147E | kap95-e126k | 0.323 | TRUE | T34E | ntf2-5001 | 0.2354 | FALSE |
| H141R | crm1_damp | 0.3199 | FALSE | G80A | yrb1-51 | 0.2354 | FALSE |
| K101R | srm1-ts | 0.3197 | TRUE | D79S | srp1-5001 | 0.2343 | FALSE |
| T34E | srm1-ts | 0.3155 | FALSE | T34G | srm1-ts | 0.2321 | FALSE |
| T34Q | ntf2-h104y | 0.3135 | FALSE | G80A | crm1_damp | 0.2317 | TRUE |
| R112A | ntf2-5001 | 0.3117 | FALSE | H141R | ntf2-5001 | 0.2296 | FALSE |
| T34E | ntf2-h104y | 0.3116 | FALSE | T34A | crm1_damp | 0.2291 | FALSE |
| R108Y | ntf2-5001 | 0.3091 | FALSE | R108I | ntf2-h104y | 0.2275 | FALSE |
| D79S | ntf2-h104y | 0.309 | FALSE | G80A | ntf2-5001 | 0.2275 | TRUE |
| D79S | srm1-ts | 0.3085 | FALSE | T34E | srm1-g282s | 0.2249 | FALSE |
| R112S | ntf2-5001 | 0.3043 | FALSE | R108Q | ntf2-h104y | 0.2245 | FALSE |
| D79S | cse1-5002 | 0.3022 | TRUE | G80A | srm1-ts | 0.2188 | FALSE |
| T34Q | srm1-ts | 0.3015 | FALSE | H141E | ma1-s116f | 0.2185 | FALSE |
| T34A | ntf2-h104y | 0.2946 | FALSE | R108L | crm1_damp | 0.2176 | TRUE |
| H141R | ntf2-h104y | 0.2929 | FALSE | D79S | ntf2-5001 | 0.2171 | FALSE |
| T34E | yrb1-51 | 0.2898 | TRUE | R108G | ntf2-h104y | 0.2171 | FALSE |
| T34A | srm1-ts | 0.2881 | FALSE | Q147E | srm1-ts | 0.2142 | FALSE |
| T34E | kap95-e126k | 0.2813 | FALSE | R108G | ntf2-5001 | 0.2131 | FALSE |
| T34A | kap95-e126k | 0.2791 | FALSE | T34A | cse1-5002 | 0.2104 | FALSE |
| R108L | srm1-ts | 0.2773 | TRUE | Q147E | ntf2-h104y | 0.2101 | FALSE |
| D79A | kap95-e126k | 0.2754 | TRUE | R108Y | srm1-ts | 0.208 | TRUE |
| H141I | crm1_damp | 0.2706 | FALSE | R112A | crm1_damp | 0.2075 | TRUE |
| T34Q | kap95-e126k | 0.2681 | FALSE | H141E | kap95-e126k | 0.2073 | FALSE |
| T34A | yrb1-51 | 0.2676 | TRUE | R108I | srm1-ts | 0.2059 | TRUE |
| T34Q | ntf2-5001 | 0.2588 | FALSE | D79A | cse1-5002 | 0.2047 | TRUE |
| Y148I | ntf2-5001 | 0.2555 | FALSE | Q147E | ntf2-5001 | 0.2044 | FALSE |
| K101R | ntf2-5001 | 0.255 | FALSE | T34Q | srm1-g282s | 0.2038 | FALSE |

Supplementary Table 4 (continued) Pearson correlations between Gsp1 mutants and the alleles of their direct interaction partners from the SGA CellMap. Ordered by correlation value.

| GSP1 mutant | Partner strain name | Pearson correlation coefficient | Residue in interface core | GSP1 mutant | Partner strain name | Pearson correlation coefficient | Residue in interface core |
|-------------|---------------------|---------------------------------|---------------------------|-------------|---------------------|---------------------------------|---------------------------|
| H141I | ntf2-h104y | 0.2025 | FALSE | Q147E | cse1-5002 | 0.148 | FALSE |
| T34E | cse1-5002 | 0.1994 | FALSE | T34G | srm1-g282s | 0.1476 | FALSE |
| R112S | srm1-ts | 0.1945 | FALSE | R108G | srm1-ts | 0.1462 | TRUE |
| Q147E | yrb1-51 | 0.1942 | FALSE | T34G | ntf2-h104y | 0.1453 | FALSE |
| R108Q | ntf2-5001 | 0.1936 | FALSE | H141E | srm1-ts | 0.1446 | FALSE |
| H141I | srm1-ts | 0.1934 | FALSE | Q147E | srp1-5001 | 0.1417 | FALSE |
| R112A | srm1-ts | 0.1929 | FALSE | R108I | srm1-g282s | 0.139 | TRUE |
| K101R | yrb1-51 | 0.1912 | FALSE | H141E | crm1_damp | 0.138 | FALSE |
| R108Q | yrb2_damp | 0.1895 | FALSE | Y148I | kap95-e126k | 0.134 | FALSE |
| R112S | crm1_damp | 0.1894 | TRUE | R112A | kap95-e126k | 0.1302 | TRUE |
| H141I | kap95-e126k | 0.188 | FALSE | T34E | ma1-1 | 0.1295 | FALSE |
| H141E | cse1-5002 | 0.1817 | FALSE | Q147E | crm1_damp | 0.1269 | FALSE |
| T34E | srp1-5001 | 0.1805 | FALSE | H141I | yrb2_damp | 0.1254 | FALSE |
| T34G | yrb1-51 | 0.1781 | TRUE | D79A | rna1-s116f | 0.1242 | FALSE |
| T34G | srp1-5001 | 0.1779 | FALSE | R108I | crm1_damp | 0.1232 | TRUE |
| G80A | srp1-5001 | 0.1775 | FALSE | T34Q | rna1-s116f | 0.1232 | FALSE |
| H141E | ntf2-5001 | 0.1762 | FALSE | R108Q | srm1-ts | 0.1214 | TRUE |
| R108L | kap95-e126k | 0.1753 | FALSE | T34A | ma1-1 | 0.1214 | FALSE |
| T34Q | cse1-5002 | 0.1738 | FALSE | T34G | ma1-1 | 0.1199 | FALSE |
| T34A | srm1-g282s | 0.1729 | FALSE | R112S | yrb2_damp | 0.1175 | FALSE |
| R108I | kap95-e126k | 0.1719 | FALSE | R108I | yrb1-51 | 0.1171 | FALSE |
| H141R | yrb2_damp | 0.1717 | FALSE | Y157A | rna1-s116f | 0.1168 | FALSE |
| D79A | srp1-5001 | 0.171 | FALSE | R108G | kap95-e126k | 0.1162 | FALSE |
| H141E | ntf2-h104y | 0.1682 | FALSE | R112S | srm1-g282s | 0.1154 | FALSE |
| D79A | yrb1-51 | 0.1672 | FALSE | H141R | kap95-e126k | 0.115 | FALSE |
| R108G | yrb2_damp | 0.1669 | FALSE | K101R | srp1-5001 | 0.1149 | TRUE |
| Y148I | yrb2_damp | 0.1654 | FALSE | Q147E | rna1-s116f | 0.1139 | FALSE |
| D79S | srm1-g282s | 0.1652 | FALSE | H141E | srp1-5001 | 0.1135 | FALSE |
| R108Y | yrb2_damp | 0.165 | FALSE | R112S | kap95-e126k | 0.1112 | TRUE |
| R108Y | kap95-e126k | 0.1645 | FALSE | D79S | rna1-s116f | 0.1081 | FALSE |
| T34A | rna1-s116f | 0.1637 | FALSE | G80A | srm1-g282s | 0.1073 | FALSE |
| D79A | ntf2-5001 | 0.1621 | FALSE | H141I | srm1-g282s | 0.1062 | FALSE |
| H141R | srm1-ts | 0.1596 | FALSE | H141I | rna1-s116f | 0.1045 | FALSE |
| T34A | srp1-5001 | 0.1557 | FALSE | R108Y | srm1-g282s | 0.104 | TRUE |
| D79A | srm1-g282s | 0.1534 | FALSE | T34G | rna1-s116f | 0.1031 | FALSE |
| T34Q | srp1-5001 | 0.1529 | FALSE | R112A | srm1-g282s | 0.1025 | FALSE |
| H141E | ma1-1 | 0.1529 | FALSE | H141E | yrb1-51 | 0.1023 | FALSE |
| R108L | srm1-g282s | 0.1527 | TRUE | T34E | rna1-s116f | 0.1013 | FALSE |
| Q147E | srm1-g282s | 0.1524 | FALSE | R112A | yrb2_damp | 0.0975 | FALSE |
| Y157A | crm1_damp | 0.1495 | TRUE | T34Q | ma1-1 | 0.0959 | FALSE |

Supplementary Table 4 (continued) Pearson correlations between Gsp1 mutants and the alleles of their direct interaction partners from the SGA CellMap. Ordered by correlation value.

| GSP1 mutant | Partner strain name | Pearson correlation coefficient | Residue in interface core | GSP1 mutant | Partner strain name | Pearson correlation coefficient | Residue in interface core |
|-------------|---------------------|---------------------------------|---------------------------|-------------|---------------------|---------------------------------|---------------------------|
| G80A | rna1-s116f | 0.0947 | FALSE | R108I | srp1-5001 | 0.0516 | FALSE |
| Y148I | srm1-ts | 0.0933 | FALSE | D79S | los1 | 0.0504 | FALSE |
| T34E | los1 | 0.0932 | FALSE | Y148I | ma1-1 | 0.0501 | FALSE |
| Y157A | kap95-e126k | 0.092 | TRUE | Y148I | srm1-g282s | 0.0482 | FALSE |
| R108L | yrb1-51 | 0.0904 | FALSE | D79A | crm1_damp | 0.0482 | TRUE |
| D79S | rna1-1 | 0.089 | FALSE | R108L | srp1-5001 | 0.047 | FALSE |
| Y157A | rna1-1 | 0.0878 | FALSE | R108I | ma1-1 | 0.045 | FALSE |
| K101R | cse1-5002 | 0.0869 | FALSE | R112S | rna1-s116f | 0.044 | FALSE |
| Y148I | rna1-s116f | 0.086 | FALSE | Q147E | los1 | 0.0436 | FALSE |
| Y157A | yrb1-51 | 0.0843 | FALSE | R112S | ma1-1 | 0.0432 | FALSE |
| H141E | yrb2_damp | 0.0828 | FALSE | R108Y | los1 | -0.0089 | TRUE |
| H141I | yrb1-51 | 0.082 | FALSE | R78K | srp1-5001 | -0.0124 | FALSE |
| R108I | msn5 | 0.0815 | TRUE | R108G | los1 | -0.0126 | TRUE |
| H141I | cse1-5002 | 0.0795 | FALSE | R78K | los1 | -0.0127 | FALSE |
| D79S | crm1_damp | 0.0789 | TRUE | R112A | cse1-5002 | -0.013 | TRUE |
| R108I | los1 | 0.075 | TRUE | Y157A | msn5 | -0.0139 | FALSE |
| T34Q | crm1_damp | 0.0745 | FALSE | R112S | los1 | -0.0142 | TRUE |
| G80A | rna1-1 | 0.0735 | FALSE | D79A | msn5 | -0.0197 | TRUE |
| T34E | crm1_damp | 0.0732 | FALSE | T34G | crm1_damp | -0.0216 | FALSE |
| R108I | cse1-5002 | 0.0721 | FALSE | H141R | ma1-1 | -0.0229 | FALSE |
| K101R | los1 | 0.0704 | FALSE | R78K | msn5 | -0.023 | FALSE |
| H141I | rna1-1 | 0.0702 | FALSE | H141I | los1 | -0.0242 | FALSE |
| R108L | los1 | 0.0699 | TRUE | H141I | msn5 | -0.0244 | FALSE |
| T34A | los1 | 0.0695 | FALSE | Y148I | msn5 | -0.0253 | FALSE |
| Q147E | rna1-1 | 0.0666 | FALSE | K101R | msn5 | -0.0271 | FALSE |
| Y148I | yrb1-51 | 0.0651 | FALSE | T34Q | yrb2_damp | -0.0272 | TRUE |
| Y157A | cse1-5002 | 0.0637 | FALSE | R108G | srp1-5001 | -0.0277 | FALSE |
| R108G | srm1-g282s | 0.0626 | TRUE | R112S | cse1-5002 | -0.0303 | TRUE |
| T34Q | los1 | 0.0616 | FALSE | R108Q | cse1-5002 | -0.0317 | FALSE |
| R108L | msn5 | 0.0612 | TRUE | R108L | rna1-s116f | -0.032 | FALSE |
| R108G | rna1-1 | 0.0609 | FALSE | Q147E | msn5 | -0.0322 | FALSE |
| Y157A | ntf2-5001 | 0.0609 | FALSE | R78K | ntf2-h104y | -0.0322 | TRUE |
| R108Q | kap95-e126k | 0.0608 | FALSE | T34E | yrb2_damp | -0.033 | TRUE |
| R108Q | msn5 | 0.0592 | TRUE | H141R | msn5 | -0.0364 | FALSE |
| H141I | srp1-5001 | 0.059 | FALSE | R108Q | rna1-s116f | -0.0378 | FALSE |
| R108G | msn5 | 0.0587 | TRUE | T34Q | msn5 | -0.0382 | FALSE |
| R108G | rna1-s116f | 0.0578 | FALSE | Y157A | srm1-g282s | -0.039 | FALSE |
| H141R | srm1-g282s | 0.0573 | FALSE | R78K | ntf2-5001 | -0.0426 | TRUE |
| D79A | rna1-1 | 0.0562 | FALSE | H141E | msn5 | -0.0441 | FALSE |
| G80A | yrb2_damp | 0.0522 | FALSE | D79S | msn5 | -0.0471 | TRUE |

Supplementary Table 4 (continued) Pearson correlations between Gsp1 mutants and the alleles of their direct interaction partners from the SGA CellMap. Ordered by correlation value.

| GSP1 mutant | Partner strain name | Pearson correlation coefficient | Residue in interface core |
|-------------|---------------------|---------------------------------|---------------------------|
| T34G | msn5 | -0.0479 | FALSE |
| R78K | kap95-e126k | -0.0485 | FALSE |
| H141R | los1 | -0.0521 | FALSE |
| R108Q | los1 | -0.0593 | TRUE |
| Y148I | los1 | -0.0601 | FALSE |
| K101R | yrb2_damp | -0.0651 | FALSE |
| R108Q | srp1-5001 | -0.0685 | FALSE |
| R108Q | yrb1-51 | -0.0696 | FALSE |
| R78K | cse1-5002 | -0.0696 | TRUE |
| R78K | rna1-1 | -0.0711 | FALSE |
| T34E | msn5 | -0.0741 | FALSE |
| R78K | yrb1-51 | -0.0814 | FALSE |
| R78K | crm1_damp | -0.0839 | TRUE |
| G80A | msn5 | -0.0892 | TRUE |

Supplementary Table 5 Interquartile range (IQR) of log2(fold change) values across all the Gsp1 mutants for each prey protein identified. Ordered by IQR.

| Prey gene name | interquartile range (IQR) | Prey gene name | interquartile range (IQR) | Prey gene name | interquartile range (IQR) |
|----------------|---------------------------|----------------|---------------------------|----------------|---------------------------|
| Spa2 | 14.10 | Scj1 | 2.44 | Rpl37a | 1.73 |
| Pup2 | 10.27 | Rtp1 | 2.44 | Svf1 | 1.72 |
| Cdc3 | 9.65 | Tub3 | 2.34 | Thi20 | 1.72 |
| Rna1 | 6.86 | Idh2 | 2.30 | Mcm6 | 1.70 |
| Mae1 | 6.34 | Idh1 | 2.20 | Npa3 | 1.70 |
| Hrp1 | 6.25 | Tub2 | 2.19 | Krs1 | 1.68 |
| Spb1 | 6.23 | Aro9 | 2.17 | Siw14 | 1.68 |
| Adr1 | 5.92 | Krr1 | 2.17 | Cbf5 | 1.67 |
| Rgr1 | 5.83 | Cia2 | 2.14 | Zuo1 | 1.67 |
| Ecm1 | 5.69 | Ade5,7 | 2.13 | Rvb1 | 1.65 |
| Swi1 | 5.66 | Ura7 | 2.08 | Wtm1 | 1.65 |
| Yar1 | 5.65 | Afg2 | 2.02 | Vps13 | 1.64 |
| Cmr1 | 5.30 | Yap1 | 2.01 | Cdc14 | 1.64 |
| Acf4 | 5.26 | Hef3 | 2.00 | Dpb4 | 1.64 |
| Vps71 | 5.25 | Hsp60 | 1.99 | Yku70 | 1.63 |
| Kri1 | 5.12 | Rpa135 | 1.98 | Fun12 | 1.62 |
| Lcp5 | 5.09 | Vps1 | 1.98 | Pwp1 | 1.61 |
| Gcd14 | 4.99 | Rvb2 | 1.96 | Rpc34 | 1.61 |
| Srp54 | 4.94 | Yrb30 | 1.96 | Aco1 | 1.60 |
| Reh1 | 4.79 | Dep1 | 1.93 | Spt8 | 1.59 |
| Gcd10 | 4.79 | San1 | 1.92 | Orc1 | 1.58 |
| Tdh1 | 4.78 | Frs1 | 1.91 | Pse1 | 1.58 |
| Srp68 | 4.75 | Rpc31 | 1.90 | Pdi1 | 1.57 |
| Srp1 | 4.61 | Oca1 | 1.90 | Rpa190 | 1.57 |
| Rpc37 | 4.04 | Mtc1 | 1.89 | Sum1 | 1.56 |
| Kap120 | 3.24 | Tti1 | 1.87 | Yku80 | 1.56 |
| Pol2 | 3.23 | Yrb1 | 1.87 | Mph1 | 1.55 |
| Kap95 | 3.05 | Ptc3 | 1.85 | Rpl26a | 1.55 |
| Rix7 | 2.93 | Sdd3 | 1.84 | Taf2 | 1.51 |
| Yef3 | 2.85 | Dbp2 | 1.80 | Net1 | 1.51 |
| Rpb8 | 2.62 | Tub1 | 1.79 | Msh2 | 1.51 |
| Gpn3 | 2.59 | Rpl39 | 1.78 | Egd1 | 1.49 |
| Rea1 | 2.56 | Swc5 | 1.78 | Rpl29 | 1.47 |
| Paa1 | 2.55 | Ugp1 | 1.77 | Hmo1 | 1.47 |
| Apa1 | 2.53 | Tif4631 | 1.77 | Tdh3 | 1.47 |
| Eno1 | 2.49 | Aim36 | 1.77 | Azf1 | 1.46 |
| Hpm1 | 2.48 | Dbp3 | 1.76 | Nop2 | 1.45 |
| Srm1 | 2.46 | Pln1 | 1.73 | Rps0b | 1.44 |

Supplementary Table 5 (continued) Interquartile range (IQR) of log₂(fold change) values across all the Gsp1 mutants for each prey protein identified. Ordered by IQR.

| Prey gene name | interquartile range (IQR) | Prey gene name | interquartile range (IQR) | Prey gene name | interquartile range (IQR) |
|----------------|---------------------------|----------------|---------------------------|----------------|---------------------------|
| Rpc82 | 1.43 | Caf40 | 1.23 | Rpo26 | 1.05 |
| Ssa1 | 1.43 | Aat1 | 1.23 | Vps72 | 1.05 |
| Gbp2 | 1.42 | Msh3 | 1.23 | Rpl30 | 1.04 |
| Lcl2 | 1.42 | Spt5 | 1.22 | Hri1 | 1.04 |
| Rpp1a | 1.41 | Rok1 | 1.22 | Nop10 | 1.03 |
| Mgm101 | 1.40 | Swr1 | 1.21 | Pdr1 | 1.03 |
| Gfa1 | 1.39 | Irc20 | 1.20 | Ald4 | 1.03 |
| Grs1 | 1.38 | Rpp2a | 1.20 | Yra1 | 1.03 |
| Mcm4 | 1.38 | Rim1 | 1.20 | Nip7 | 1.02 |
| Puf6 | 1.38 | Hpc2 | 1.19 | Prp43 | 1.02 |
| Rpl10 | 1.37 | Mcm5 | 1.19 | Rtt106 | 1.02 |
| Tra1 | 1.37 | Rpl15a | 1.19 | Hir2 | 1.02 |
| Pro3 | 1.37 | Rpa49 | 1.19 | Arp5 | 1.02 |
| Nop4 | 1.35 | Ret1 | 1.18 | Itc1 | 1.02 |
| Tfc3 | 1.35 | Tkl2 | 1.17 | Rpc40 | 1.01 |
| Spt20 | 1.35 | Hst1 | 1.16 | Ade3 | 1.01 |
| Rpl3 | 1.34 | Rpl9a | 1.16 | Hho1 | 1.01 |
| Rpl33b | 1.33 | Elo1 | 1.16 | Rpl5 | 1.00 |
| Cdc9 | 1.33 | Rtg3 | 1.16 | Stm1 | 1.00 |
| Ubp15 | 1.32 | Rfm1 | 1.15 | Reb1 | 1.00 |
| Rpc11 | 1.31 | Gdh1 | 1.14 | loc4 | 0.99 |
| Rpo21 | 1.31 | Sry1 | 1.13 | Asg1 | 0.99 |
| Rlp24 | 1.31 | Chd1 | 1.12 | loc3 | 0.99 |
| Skn7 | 1.31 | Top2 | 1.11 | Msn1 | 0.99 |
| Hsp42 | 1.31 | Rpl31b | 1.11 | Adh6 | 0.99 |
| Cys4 | 1.30 | Cst6 | 1.11 | Rpc19 | 0.99 |
| Orc2 | 1.30 | Rpl36a | 1.10 | Rpc53 | 0.98 |
| Hca4 | 1.29 | Rpl4a | 1.10 | Adh3 | 0.98 |
| Ree1 | 1.29 | Abf2 | 1.09 | Rbg1 | 0.98 |
| Ssz1 | 1.27 | Rpb5 | 1.09 | Raf1 | 0.98 |
| Yta7 | 1.27 | Spt7 | 1.08 | Orc3 | 0.98 |
| Pre6 | 1.26 | Orc4 | 1.08 | Rfc1 | 0.96 |
| Gtr2 | 1.26 | Sin3 | 1.08 | Srl2 | 0.96 |
| Hal5 | 1.25 | Rpo31 | 1.07 | Rpl24a | 0.96 |
| Rpb4 | 1.24 | Nur1 | 1.07 | Top1 | 0.95 |
| Nop6 | 1.24 | Rpb10 | 1.06 | Rpl6b | 0.95 |
| Rpc25 | 1.23 | Sko1 | 1.06 | Isw1 | 0.95 |
| Muk1 | 1.23 | Rpp2b | 1.06 | Sth1 | 0.94 |

Supplementary Table 5 (continued) Interquartile range (IQR) of log₂(fold change) values across all the Gsp1 mutants for each prey protein identified. Ordered by IQR.

| Prey gene name | interquartile range (IQR) | Prey gene name | interquartile range (IQR) | Prey gene name | interquartile range (IQR) |
|----------------|---------------------------|----------------|---------------------------|----------------|---------------------------|
| Nhp2 | 0.94 | Cdc1 | 0.72 | Slx9 | 0.00 |
| Egd2 | 0.93 | Pob3 | 0.69 | Smc2 | 0.00 |
| Npl6 | 0.90 | Htz1 | 0.68 | Snf12 | 0.00 |
| Rps29a | 0.90 | Spt15 | 0.68 | Snf5 | 0.00 |
| Taf9 | 0.89 | Rsc58 | 0.67 | Spp41 | 0.00 |
| Gar1 | 0.89 | Hir1 | 0.64 | Stb4 | 0.00 |
| Rsc4 | 0.89 | Rfc3 | 0.62 | Sti1 | 0.00 |
| Snf2 | 0.88 | Hos3 | 0.61 | Sub1 | 0.00 |
| Taf14 | 0.88 | Mot1 | 0.61 | Tif4632 | 0.00 |
| Grx1 | 0.87 | Rsc8 | 0.61 | | |
| Rpl8b | 0.87 | Arp4 | 0.60 | | |
| Rsc6 | 0.87 | Pre2 | 0.60 | | |
| Mog1 | 0.86 | Ies2 | 0.60 | | |
| Rsc9 | 0.84 | Arp7 | 0.55 | | |
| Rsc3 | 0.84 | Rpc10 | 0.54 | | |
| Gcd1 | 0.83 | Ant1 | 0.54 | | |
| Rfc2 | 0.83 | Abf1 | 0.54 | | |
| Swi3 | 0.83 | Thi7 | 0.52 | | |
| Ies5 | 0.82 | Lsm6 | 0.51 | | |
| loc2 | 0.82 | Rfc5 | 0.49 | | |
| Imh1 | 0.81 | Hir3 | 0.49 | | |
| Oye2 | 0.80 | Srp14 | 0.48 | | |
| Ies1 | 0.80 | Rco1 | 0.45 | | |
| Nhp10 | 0.79 | Rfc4 | 0.43 | | |
| Arp9 | 0.79 | Aim14 | 0.37 | | |
| Spt16 | 0.77 | Sis1 | 0.33 | | |
| Sfh1 | 0.76 | Aah1 | 0.00 | | |
| Htb2 | 0.76 | Aim41 | 0.00 | | |
| Enp2 | 0.76 | Arl3 | 0.00 | | |
| Taf10 | 0.76 | Cfd1 | 0.00 | | |
| Bur6 | 0.76 | Gcn3 | 0.00 | | |
| Isw2 | 0.75 | Lrs4 | 0.00 | | |
| Rsc2 | 0.75 | Opi1 | 0.00 | | |
| Taf5 | 0.74 | Rad5 | 0.00 | | |
| Ies3 | 0.74 | Rpl21b | 0.00 | | |
| Rpb11 | 0.74 | Rrp8 | 0.00 | | |
| Arp8 | 0.73 | Rrs1 | 0.00 | | |
| Rtt102 | 0.73 | Sen1 | 0.00 | | |

Supplementary Table 6 Michaelis-Menten parameters of GAP-mediated GTP hydrolysis. The two Michaelis-Menten parameters and their ratio (enzymatic efficiency) are determined by an integrated Michaelis-Menten fit for each individual experiment. Standard error is based on three or more replicates.

| Gsp1 mutant | k _{cat} [s ⁻¹] | std.error k _{cat} [s ⁻¹] | K _m [μM] | std.error K _m [μM] | k _{cat} /K _m [s ⁻¹ μM ⁻¹] | std.error k _{cat} /K _m [s ⁻¹ μM ⁻¹] |
|-------------|-------------------------------------|---|---------------------|-------------------------------|--|--|
| WT | 9.2 | 0.66 | 0.4 | 0.04 | 26.0 | 2.57 |
| T34A | 9.8 | 3.65 | 2.3 | 0.63 | 4.0 | 0.56 |
| T34E | 8.9 | 0.23 | 1.4 | 0.09 | 6.5 | 0.36 |
| T34G | 5.0 | 0.81 | 0.8 | 0.12 | 7.1 | 0.99 |
| T34L | 15.2 | 1.27 | 2.0 | 0.10 | 7.5 | 0.88 |
| T34Q | 5.4 | 0.20 | 2.2 | 0.26 | 2.5 | 0.23 |
| F58A | 8.6 | 0.57 | 0.2 | 0.03 | 35.8 | 2.97 |
| R78K | 4.3 | 0.73 | 2.1 | 0.59 | 2.4 | 0.35 |
| D79A | 11.9 | 2.21 | 3.6 | 1.11 | 3.8 | 0.62 |
| D79S | 4.1 | 0.32 | 1.7 | 0.23 | 3.0 | 0.59 |
| G80A | 8.8 | 0.14 | 0.3 | 0.01 | 28.8 | 1.56 |
| K101R | 8.2 | 1.22 | 0.2 | 0.01 | 44.7 | 9.20 |
| R108A | 7.8 | 0.32 | 0.2 | 0.01 | 42.0 | 4.14 |
| R108G | 9.2 | 0.16 | 0.1 | 0.01 | 82.3 | 5.74 |
| R108I | 13.2 | 2.24 | 3.1 | 0.66 | 4.3 | 0.15 |
| R108L | 5.2 | 0.63 | 0.3 | 0.07 | 19.3 | 2.87 |
| R108Q | 9.2 | 0.03 | 0.2 | 0.00 | 61.2 | 1.18 |
| R108Y | 7.8 | 1.39 | 0.2 | 0.07 | 40.1 | 6.34 |
| R112S | 4.9 | 1.28 | 3.0 | 1.01 | 1.7 | 0.20 |
| K132H | 6.7 | 0.45 | 5.6 | 0.13 | 1.2 | 0.06 |
| H141R | 7.2 | 1.19 | 0.1 | 0.02 | 56.3 | 3.04 |
| K143W | 9.5 | 0.86 | 0.1 | 0.02 | 71.8 | 3.48 |
| Q147E | 7.6 | 0.65 | 0.7 | 0.04 | 11.6 | 1.58 |
| Y157A | 8.8 | 1.89 | 0.2 | 0.03 | 57.7 | 4.87 |
| A180T | 4.0 | 0.49 | 0.4 | 0.04 | 11.1 | 0.29 |

Supplementary Table 7 Michaelis-Menten parameters of GEF-mediated nucleotide exchange.

Standard error is based on the error of the Michaelis-Menten fit to the data.

| Gsp1 mutant | k_{cat} [s^{-1}] | std.error k_{cat} [s^{-1}] | K_m [μM] | std.error K_m [μM] | k_{cat}/K_m [$s^{-1} \mu M^{-1}$] | std.error k_{cat}/K_m [$s^{-1} \mu M^{-1}$] |
|----------------|------------------------|-------------------------------------|-------------------|--------------------------------|--|---|
| WT | 3.0 | 0.08 | 0.9 | 0.12 | 3.3 | 0.44 |
| T34A | 1.8 | 0.10 | 0.9 | 0.22 | 2.1 | 0.55 |
| T34E | 1.7 | 0.07 | 1.0 | 0.17 | 1.7 | 0.29 |
| T34G | 2.5 | 0.14 | 1.4 | 0.28 | 1.8 | 0.39 |
| T34L | 2.0 | 0.11 | 1.6 | 0.35 | 1.2 | 0.27 |
| T34Q | 1.3 | 0.05 | 1.0 | 0.14 | 1.3 | 0.20 |
| F58A | 1.9 | 0.06 | 1.6 | 0.16 | 1.2 | 0.13 |
| R78K | 3.5 | 0.19 | 10.2 | 1.43 | 0.3 | 0.05 |
| D79A | 3.2 | 0.14 | 2.6 | 0.31 | 1.2 | 0.15 |
| D79S | 2.2 | 0.12 | 0.9 | 0.21 | 2.6 | 0.64 |
| G80A | 1.2 | 0.10 | 1.0 | 0.33 | 1.2 | 0.39 |
| K101R | 4.0 | 0.42 | 304.9 | 50.52 | 0.0 | 0.00 |
| R108A | 3.0 | 0.13 | 0.9 | 0.16 | 3.2 | 0.56 |
| R108G | 5.4 | 0.12 | 8.5 | 0.55 | 0.6 | 0.04 |
| R108I | 8.1 | 0.55 | 149.2 | 15.73 | 0.1 | 0.01 |
| R108L | 3.4 | 0.08 | 49.2 | 2.95 | 0.1 | 0.00 |
| R108Q | 3.8 | 0.10 | 8.7 | 0.64 | 0.4 | 0.03 |
| R108Y | 4.5 | 0.14 | 19.3 | 1.59 | 0.2 | 0.02 |
| R112S | 0.8 | 0.12 | 4.1 | 1.28 | 0.2 | 0.07 |
| K132H | 1.9 | 0.17 | 1.6 | 0.49 | 1.1 | 0.35 |
| H141R | 0.6 | 0.03 | 0.5 | 0.13 | 1.2 | 0.30 |
| K143W | 1.2 | 0.08 | 0.6 | 0.20 | 1.8 | 0.57 |
| Q147E | 1.9 | 0.07 | 1.4 | 0.18 | 1.4 | 0.19 |
| Y157A | 1.0 | 0.06 | 1.0 | 0.24 | 0.9 | 0.22 |
| A180T | 2.3 | 0.05 | 1.2 | 0.09 | 2.0 | 0.16 |

Supplementary Table 8 Intrinsic GTP hydrolysis rate of wild type and mutant Gsp1. Standard deviation is based on data from 3 or more replicates.

| Gsp1 mutant | intrinsic GTP hydrolysis rate [s ⁻¹] | std.error of intrinsic GTP hydrolysis rate [s ⁻¹] |
|-------------|--|---|
| WT | 2.5E-05 | 1.2E-06 |
| T34A | 7.4E-06 | 3.0E-06 |
| T34E | 8.7E-06 | 1.1E-06 |
| T34G | 2.0E-05 | 1.9E-06 |
| T34L | 1.8E-05 | 3.7E-07 |
| T34Q | 6.6E-06 | 3.0E-06 |
| F58A | 2.1E-05 | 2.7E-07 |
| R78K | 8.0E-06 | 3.9E-06 |
| D79A | 4.3E-05 | 1.2E-05 |
| D79S | 1.8E-05 | 2.9E-06 |
| G80A | 1.5E-05 | 7.3E-07 |
| K101R | 2.7E-05 | 2.1E-06 |
| R108A | 1.4E-05 | 4.9E-07 |
| R108G | 1.9E-05 | 1.2E-06 |
| R108I | 3.4E-05 | 8.8E-06 |
| R108L | 1.9E-05 | 9.4E-07 |
| R108Q | 1.9E-05 | 5.0E-07 |
| R108Y | 2.0E-05 | 2.4E-06 |
| R112S | 1.6E-05 | 5.9E-06 |
| K132H | 3.3E-05 | 4.9E-06 |
| H141R | 3.1E-05 | 8.8E-07 |
| K143W | 2.9E-05 | 7.6E-07 |
| Q147E | 1.6E-05 | 9.6E-08 |
| Y157A | 3.9E-05 | 5.5E-06 |
| A180T | 2.7E-05 | 1.4E-06 |

Supplementary Table 9 Apparent T_m values estimated from the circular dichroism (CD) thermal melts. Mutants are ordered by apparent T_m.

| Gsp1 mutant | Apparent Tm / °C |
|-------------|------------------|
| R78K | 79 |
| G80A | 77 |
| T34G | 77 |
| R108Y | 77 |
| N105L | 77 |
| R108G | 77 |
| WT | 76 |
| T34L | 76 |
| K101R | 76 |
| R108Q | 75 |
| R108I | 74 |
| A180T | 74 |
| K132H | 74 |
| Q147E | 73 |
| R108L | 73 |
| K143W | 73 |
| D79S | 72 |
| R112S | 71 |
| H141I | 66 |
| H141V | 63 |
| H141R | 63 |
| Y157A | 63 |

Titles and Legends of Supplementary Source Files

Source File 1 Genetic interaction (GI) data from the E-MAP screens.

This source file contains genetic interaction (GI) scores (S-scores) from the E-MAP screens of 56 *S. cerevisiae* strains (wild type and 55 Gsp1 point mutants).

Table column names:

query allele name (Gsp1 mutant): point mutation (amino acid substitution) in the *S. cerevisiae* Gsp1 gene (query gene in the E-MAP screen, see Methods and Ref.²³).

query allele ORF: open reading frame ID, a unique database identifier of the query gene Gsp1 (from the Saccharomyces Genome Database, yeastgenome.org).

array allele: allele name, either a gene deletion or a gene DAmP²⁴ (array gene in the E-MAP screen, see Methods and Ref.²³).

array allele ORF: open reading frame ID, a unique database identifier of the array gene (from the Saccharomyces Genome Database, yeastgenome.org).

E-MAP S-score: genetic interaction (GI) score between the query and the array alleles. See Refs. ^{5,23,24} for definition.

Source File 2 Pairwise Pearson correlations of profiles between SGA genes and Gsp1 point mutants, with associated p-values.

This source file contains the Pearson correlation coefficients and accompanying p-values for correlations between genetic interaction profiles of Gsp1 point mutants and the genetic interaction profiles of *S. cerevisiae* alleles from the CellMap SGA dataset published in ¹⁴.

Table column names:

mutant: point mutation (amino acid substitution) in the *S. cerevisiae* Gsp1 gene (query gene in the E-MAP screen).

CellMAP_allele: *S. cerevisiae* gene allele (gene deletion) from the CellMap ^{14,53}.

yeast_gene: standard gene name (as defined in the Saccharomyces Genome Database, yeastgenome.org) of the CellMap allele.

Pearson correlation: Pearson correlation between the genetic interaction profile of a Gsp1 mutant and the CellMAP allele (from the dataset from Ref.^{14,53}).

greater p-value: p-value associated with the Pearson correlation (one-sided positive t-test).

greater FDR: greater p-value after correction by the FDR method.

greater Bonferroni: greater p-value after Bonferroni correction.

Source File 3 Affinity purification mass spectrometry (AP-MS) data reported as fold change and significance value, as well as a list of significant interaction hits.

This source file contains two tables:

Table 1 contains the affinity purification mass spectrometry (AP-MS) data for Gsp1 point mutants. The data in the table are the output from MSstats³⁵ (see Supplementary Methods) and report on the abundance of the pulled down protein, the log-transformed fold change of the abundance compared to the wild type with the appropriate 3xFLAG tag, and the accompanying FDR adjusted p-value. The data are provided for both the global and equalized median normalization methods available.

Table column names:

sample: unique identifier of the *S. cerevisiae* strain. Contains information on the position of the 3xFLAG tag (N- or C-terminal) and the point mutation (amino acid substitution) in the GSP1 gene.

terminus position of the 3xFLAG tag: N- or C-terminus position of the 3xFLAG tag.

Gsp1 mutant: amino acid substitution in the GSP1 gene in *S. cerevisiae*.

normalization method (equalized median or global standard of PPI list): normalization method used in MSstats (eqM is equalized median, gs is global standard).

Prey protein ORF: open reading frame ID, a unique database identifier of the pulled-down protein interaction partner in the AP-MS experiment with Gsp1 point mutants (ORF ID defined in the Saccharomyces Genome Database, yeastgenome.org).

Prey protein gene name: standard gene name of the pulled-down protein interaction partner (as defined in the Saccharomyces Genome Database, yeastgenome.org).

log₂ (fold change): log-transformed fold change of the abundance of pulled-down interaction partner between the point mutant and the wild type Gsp1 sample with the corresponding 3xFLAG tag (N- or C-terminal).

FDR adjusted p-value: FDR adjusted p-value of the fold change of abundance, from MSstats.

abundance of pulled down protein: total abundance of the pulled-down protein interaction partner.

Table 2 contains the list of high-confidence interaction partners of Gsp1 from our AP-MS experiments (as determined by SAINTexpress³⁴, see Supplementary Methods).

Table column names:

C-terminal 3xFLAG tag: list of high-confidence protein interaction partners identified with wild type or mutant Gsp1 with the C-terminal 3xFLAG tag.

N-terminal 3xFLAG tag: list of high-confidence protein interaction partners identified with wild type or mutant Gsp1 with the N-terminal 3xFLAG tag.

ORF: open reading frame ID, a unique database identifier of the gene (as defined in the Saccharomyces Genome Database, yeastgenome.org)

gene name: standard gene name (as defined in the Saccharomyces Genome Database, yeastgenome.org)

Source File 4 *S. cerevisiae* genes from the SGA data with significant positive correlations with Gsp1 mutants organized by biological functions into gene sets.

This file provides a list of *S. cerevisiae* alleles from the SGA dataset whose GI profiles have significant correlations with the GI profiles of Gsp1 mutants (see Methods). The genes were manually grouped into “gene sets” based on their biological function (as annotated in the Saccharomyces Genome Database, yeastgenome.org).

Table column names:

Allele in the SGA CellMAP: *S. cerevisiae* gene allele (gene deletion) from the CellMap^{14,53}.

S. cerevisiae gene name: standard gene name of the CellMap allele (as defined in the Saccharomyces Genome Database, yeastgenome.org).

gene set: annotated gene set (genes grouped by their annotated biological function from the Saccharomyces Genome Database, yeastgenome.org, and updated annually).

Cluster from Fig. 4a (1-7, or expanded dataset, see Methods): cluster number (1-7) corresponding to the hierarchical clustering presented in Fig. 4a.

Supplementary References

- 42 Braberg, H. *et al.* Quantitative analysis of triple-mutant genetic interactions. *Nature protocols* **9**, 1867-1881, doi:10.1038/nprot.2014.127 (2014).
- 43 Murtagh, F. & Legendre, P. Ward's Hierarchical Agglomerative Clustering Method: Which Algorithms Implement Ward's Criterion? *Journal of Classification* **31**, 274-295, doi:10.1007/s00357-014-9161-z (2014).
- 44 Becker, J. *et al.* RNA1 encodes a GTPase-activating protein specific for Gsp1p, the Ran/TC4 homologue of *Saccharomyces cerevisiae*. *The Journal of biological chemistry* **270**, 11860-11865 (1995).
- 45 Klebe, C., Prinz, H., Wittinghofer, A. & Goody, R. S. The Kinetic Mechanism of Ran-Nucleotide Exchange Catalyzed by RCC1. *Biochemistry* **34**, 12543-12552, doi:10.1021/bi00039a008 (1995).
- 46 Gideon, P. *et al.* Mutational and kinetic analyses of the GTPase-activating protein (GAP)-p21 interaction: the C-terminal domain of GAP is not sufficient for full activity. *Molecular and Cellular Biology* **12**, 2050-2056, doi:10.1128/MCB.12.5.2050 (1992).
- 47 Brinkmann, T. *et al.* Rap-specific GTPase Activating Protein follows an Alternative Mechanism. *Journal of Biological Chemistry* **277**, 12525-12531, doi:10.1016/S1097-2765(01)80010-1 (2002).
- 48 Schnell, S. Validity of the Michaelis-Menten equation - steady-state or reactant stationary assumption: that is the question. *The FEBS journal* **281**, 464-472, doi:10.1023/A:1019139423811 (2013).
- 49 Hanson, S. M. & Schnell, S. Reactant Stationary Approximation in Enzyme Kinetics. *J Phys Chem A* **112**, 8654-8658, doi:10.1021/jp8026226 (2008).
- 50 Tien, M. Z., Meyer, A. G., Sydykova, D. K., Spielman, S. J. & Wilke, C. O. Maximum allowed solvent accessibilites of residues in proteins. *PLoS One* **8**, e80635, doi:10.1371/journal.pone.0080635 (2013).
- 51 Grant, B. J., Rodrigues, A. P. C., ElSawy, K. M., McCammon, J. A. & Caves, L. S. D. Bio3d: an R package for the comparative analysis of protein structures. *Bioinformatics* **22**, 2695-2696, doi:10.1093/bioinformatics/btl461 (2006).
- 52 Gu, Z., Eils, R. & Schlesner, M. Complex heatmaps reveal patterns and correlations in multidimensional genomic data. *Bioinformatics* **32**, 2847-2849, doi:10.1093/bioinformatics/btw313 (2016).
- 53 Usaj, M. *et al.* TheCellMap.org: A Web-Accessible Database for Visualizing and Mining the Global Yeast Genetic Interaction Network. *G3* **7**, 1539-1549, doi:10.1534/g3.117.040220 (2017).
- 54 Ryan, C. J. *et al.* Hierarchical Modularity and the Evolution of Genetic Interactomes across Species. *Molecular Cell* **46**, 691-704, doi:10.1016/j.molcel.2012.05.028 (2012).
- 55 Smith, S. J. M. & Rittinger, K. Preparation of GTPases for Structural and Biophysical Analysis. *Methods in Molecular Biology* **189**, 013-024, doi:10.1385/1-59259-281-3:013 (2002).
- 56 Seewald, M. J. *et al.* Biochemical Characterization of the Ran-RanBP1-RanGAP System: Are RanBP Proteins and the Acidic Tail of RanGAP Required for the Ran-RanGAP GTPase Reaction? *Molecular and Cellular Biology* **23**, 8124-8136, doi:10.1128/MCB.23.22.8124-8136.2003 (2003).